Please cite this paper as:

Zhu Z, Zhu S, Wong YW and Ni YQ (2023) Structural dynamic response reconstruction with multi-type sensors, unknown input, and rank deficient feedthrough matrix. *Mechanical Systems and Signal Processing*. 187: 109935.
https://doi.org/10.1016/j.ymssp.2022.109935

Structural Dynamic Response Reconstruction with Multi-type Sensors, Unknown Input, and Rank Deficient Feedthrough Matrix

Zimo ZHU, Songye ZHU*, You-Wu WANG, Yi-Qing NI

[a] Department of Civil and Environmental Engineering, The Hong Kong Polytechnic University, Hong Kong, China.

* Corresponding author: Songye Zhu, Email: songye.zhu@polyu.edu.hk

ABSTRACT:

This paper presents a novel algorithm that reconstructs structural responses under unknown inputs and rank-deficient feedthrough matrix conditions. The algorithm eliminates one of the major constraints of existing filters (i.e., the requirement of a full-rank matrix), allowing the number of accelerometers required in real applications to be reduced. A unified linear input and state estimator (ULISE) is introduced into structural response reconstruction for the first time. The ULISE requires no prior assumptions on the time histories of unknown inputs. The direct feedthrough matrix can either be rank-deficient or full-column-rank. Moreover, the ULISE eliminates the time delay problem in the input reconstruction based on displacement measurement. The effectiveness of the proposed ULISE-based structural response reconstruction algorithm is evaluated and validated through numerical simulations and laboratory tests. The proposed algorithm achieves reasonable joint input–state estimation even under rank-deficient feedthrough matrix conditions and can be regarded as a generalized and improved version of the existing response reconstruction filters.

KEYWORDS:

Optimal filtering, Response reconstruction, Input estimation, Unknown input, Sensor data fusion

1. Introduction

Structural health monitoring (SHM) techniques have rapidly advanced over the past several decades. SHM is widely used to provide information on in-service civil structures and ensure their operational safety [1, 2]. An effective SHM system is expected to provide accurate measurements of structural responses and external loadings. The sensor network is one of the most important components of SHM systems and usually accounts for a sizeable share of the budget. However, placing sensors on all degrees of freedom (DOFs) of large-scale civil structures is neither realistic nor necessary. Accessibility and constructability also affect sensor installation and measurement. Therefore, it is too ambitious to measure all environmental excitations, particularly distributed excitations (e.g., wind loads). Consequently, reconstructing structural dynamic responses with unknown inputs based on only partial observations is an inevitable but challenging task in the SHM of civil structures.

Structural response reconstruction under known input loads has widely been explored, and various algorithms have been proposed to meet the needs in different cases. For example, in 1997, Kammer [3] proposed a response reconstruction technique based on transmissibility. Transmissibility was defined as the ratio of the response to the harmonic excitation amplitude. In 1998, Ewins and Liu [4] extended this method to a multi-DOF system in the frequency domain. However, given that the transmissibility-based method is a frequency domain method, the real-time reconstruction of structural responses in the time domain is difficult, and such reconstruction is frequently required in the SHM of civil structures.

The empirical mode decomposition (EMD)-based method is a time-domain response reconstruction technique applicable to nonlinear and nonstationary processes [5]. He et al. [6] presented an EMD method with intermittency criteria and transformation equations derived from a finite element (FE) model. The EMD-based method highly depends on the accuracy of the FE model to obtain the baseline data. However, its readiness for applications in large civil structures remains unknown. Another algorithm that was developed several decades ago is the inverse optimization-based method, in which the reconstruction problem is defined as an inverse optimization problem subject to constraints. Ambrosino [7] and Setola [8] first used this method in the response reconstruction of civil structures in the 1990s. In 2003, the algorithm was further developed by Limongelli [9]. This method gradually lost popularity owing to the computational cost required in the optimization process. Moreover, representing real structures using simple functions is often challenging.

Seeking computational-friendly methods suitable for sophisticated civil structures is a promising

future research direction. The state-space representation of a specific structure is a mathematical model that relates input, output, and state variables through first-order differential equations. State estimation can be realized using various filters. Kalman [10] first proposed the Kalman filter (KF) in 1960. In 2013, Zhu et al. [11] presented a KF-based structural response reconstruction technique. Using the normalization procedure, researchers have achieved data fusion for acceleration, displacement, and strain measurements [12, 13]. Higher modes can be truncated to simplify calculations for large-scale structures. Xu et al. [14] successfully applied the mode selection algorithm to the SHM of long-span suspension bridges. Considering that both the process and observation models can produce nonlinearities, the extended KF (EKF) can linearize the state vector and covariance matrix around the current estimate; thus, it can be regarded as the nonlinear version of KF. In 1984, Hoshiya [15] proposed the use of an EKF for solving the seismic structural system identification problem. Lei et al. [16] presented an adaptive EKF approach to track changes in structural parameters, including stiffness, damping, and unknown inputs. The EKF loses its priorities when simulating non-Gaussian processes, and the computation of the Jacobian matrix in EKF for complex civil structures is also quite demanding.

In real-world applications, the direct monitoring of external excitations may be impossible. Unknown excitations are sometimes assumed to be Gaussian processes (e.g. [17]) to allow for the estimation of the structural state. KF-based response reconstruction for linear time-invariant systems subject to unknown input loads has attracted considerable attention in the field of system identification without preliminary information on unknown excitation. The filters can be divided into two classes according to the estimation sequences for state and input. In the first class, an augmented state vector is defined by including the input vectors. The state and unknown inputs can therefore be estimated simultaneously, and the estimation can then be solved as a conventional KF problem. Lourens et al. [18] proposed an augmented KF (AKF) for unknown force identification in structural systems. The presented algorithm allowed for the concurrent reconstruction of the state and the input. Aucejo et al. [19] demonstrated the advantages and disadvantages of the AKF in the purely input estimation process. Naets et al. [20] analytically investigated the stability of the AKF for the estimation of unknown inputs and states and reported that the use of accelerometers might compromise result reliability. Dertimanis et al. [21] combined the unscented KF and AKF to achieve input–state–parameter estimation through partial observations. Recently, Tatsis et al. [22] performed structural crack detection using the AKF and the Bayesian approach. The second class of filters separately considers the input and state in the estimation

problem. Kitanidis [23] developed the first optimal recursive state filter that included no assumptions regarding the unknown input. Hsieh [24] derived a two-stage filter based on Kitanidis's recursive filter that can estimate the unknown input. In 2007, Gillijns and De Moor proved the optimality of unbiased minimum-variance input estimation [25]. The authors further extended the algorithm to a system with a full-rank direct feedthrough matrix in [26]. In 2012, Lourens et al. introduced the method to structural dynamic response reconstruction for reduced-order models [27]. Maes et al. [28] further extended the abovementioned algorithm to applications with unknown stochastic excitations. Maes et al. [29] reduced the estimation uncertainties in the input–state estimation process through a smoothing procedure.

Currently, most of the structural response reconstruction techniques under unknown inputs are based on the Gillijns and De Moor filter (GDF) [26]. In the GDF-based dynamic response reconstruction, the state vector comprises structural displacement and velocity. Two versions of GDF methods have been developed. The first version, denoted as GDF-I, is without an input feedthrough matrix in the observation equation [25]. It should be adopted when only displacement-related measurements (displacement or strain) and/or velocity measurements are available. The acceleration measurements shall be disregarded to apply this filter. The second version, denoted as GDF-II, corresponds to a system with a full-column-rank feedthrough matrix in the observation matrix [26]. From the perspective of structural dynamics, this approach requires accelerations are recorded, and the number of accelerometers must be greater than or at least equal to the number of unknown inputs [30]. For distributed excitations (e.g., wind loads), many accelerometers need to be installed to fulfill the full rank requirement. As accelerometers are commonly installed in SHM systems, GDF-II [26] forms the basis of most of the current response reconstruction algorithms with unknown inputs. In the present study, the algorithm GDF-II is considered for comparison.

However, the two aforementioned GDF algorithms have limitations in solving dynamic response reconstruction problems. (1) The GDF-I algorithm, which is without an input feedthrough matrix, features time delay. Given a system with a measured displacement or strain at time k, only the input at time $k-1$ can be estimated owing to the absence of the input feedthrough matrix, which means that the state at time k must be estimated without any input knowledge. Moreover, acceleration measurements are disregarded in GDF-I. (2) The second algorithm, GDF-II [26], requires the direct feedthrough matrix to be full rank in the presence of accelerometers. This condition increases the required number and cost

of accelerometers and complicates the reconstruction of distributed loads. Presently, structural dynamic response reconstruction using a rank-deficient feedthrough matrix remains a challenge. (3) Acceleration and displacement measurement data contain the input information at time k and k-1, respectively. Although the GDF-II algorithm can combine both data, displacement and acceleration measurements cannot be directly fused for input estimation at time k.

In this study, a state-of-the-art response reconstruction method for structures subjected to unknown input loads is developed using a unified linear input and state estimator (ULISE) [31] to overcome the aforementioned deficiencies. The ULISE algorithm was recently developed for systems without a full rank feedthrough matrix, and it is based on minimum-variance unbiased optimization. However, to the best of the authors' knowledge, the application of ULISE in structural response reconstruction has not been reported thus far. The normalization technique is also adopted to solve the ill-conditioned problem in multi-type sensor data fusion. In addition to displacement and acceleration, strain measurement is incorporated by considering structural shape functions. No assumption regarding the excitation time histories is made, which allows for the application of this method to different scenarios. The direct feedthrough matrix in the observation equation can be either full-column-rank or rank-deficient. Partially observed systems and non-collocated monitoring are allowed in the proposed ULISE algorithm. The proposed method allows the number of accelerometers and the sensor network costs to be reduced. The proposed method is a generalized and improved version of the existing GDF-based response reconstruction techniques and has great application potential.

The remainder of the paper is organized as follows. Section 2 presents the state-space mathematical formulation of a dynamic structural system. Section 3 discusses the ULISE algorithm and normalization technique. Section 4 presents numerical studies on the proposed algorithm and compares the algorithm with the traditional GDF-based method. Section 5 describes the verification of the algorithm effectiveness via laboratory experiments on a shear frame.

2. Formulation of the structural dynamics problem

2.1 Equations of motion

A second-order differential equation is commonly used in the dynamic modeling of an n DOF linear structural system.

$$\mathbf{M}\ddot{\mathbf{z}}(t)+\mathbf{C}\dot{\mathbf{z}}(t)+\mathbf{K}\mathbf{z}(t)=\mathbf{S}_{\mathrm{d}}\mathbf{d}(t) \tag{1}$$

where $\mathbf{z}(t)\in\mathbb{R}^{n_{DOF}}$ is the nodal displacement vector; $\mathbf{M}\in\mathbb{R}^{n_{DOF}\times n_{DOF}}$, $\mathbf{C}\in\mathbb{R}^{n_{DOF}\times n_{DOF}}$, and $\mathbf{K}\in\mathbb{R}^{n_{DOF}\times n_{DOF}}$ denote the mass, damping, and stiffness matrices, respectively; $\mathbf{d}(t)\in\mathbb{R}^{n_{\mathrm{d}}}$ is the external load vector applied to the structural system; $\mathbf{S}_{\mathrm{d}}\in\mathbb{R}^{n_{DOF}\times n_{\mathrm{d}}}$ is the spatial distribution matrix for the external load, in which the nonzero entries relate the load and the corresponding DOFs.

2.2 State-space model

The state vector $\mathbf{x}(t)=\begin{Bmatrix}\mathbf{z}(t)\\ \dot{\mathbf{z}}(t)\end{Bmatrix}$ is defined by combining the nodal displacement and velocity vectors. Then, the second-order differential expression in Eq. (1) can be rewritten in a state-space form as

$$\dot{\mathbf{x}}(t)=\mathbf{A}_{\mathrm{c}}\mathbf{x}(t)+\mathbf{G}_{\mathrm{c}}\mathbf{d}(t) \tag{2}$$

$$\mathbf{y}(t)=\mathbf{C}_{\mathrm{c}}\mathbf{x}(t)+\mathbf{H}_{\mathrm{c}}\mathbf{d}(t) \tag{3}$$

where the system matrix $\mathbf{A}_{\mathrm{c}}\in\mathbb{R}^{2n_{DOF}\times 2n_{DOF}}$ and the input matrix $\mathbf{G}_{\mathrm{c}}\in\mathbb{R}^{2n_{DOF}\times n_{\mathrm{d}}}$ can be expressed as

$$\mathbf{A}_{\mathrm{c}}=\begin{bmatrix}\mathbf{0}_{n_{DOF}} & \mathbf{I}_{n_{DOF}}\\ -\mathbf{M}^{-1}\mathbf{K} & -\mathbf{M}^{-1}\mathbf{C}\end{bmatrix},\quad \mathbf{G}_{\mathrm{c}}=\begin{bmatrix}\mathbf{0}_{n_{DOF}}\\ \mathbf{M}^{-1}\mathbf{S}_{\mathrm{d}}\end{bmatrix} \tag{4}$$

Eq. (3) is the observation equation, in which $\mathbf{C}_{\mathrm{c}}\in\mathbb{R}^{n_{\mathrm{y}}\times 2n_{\mathrm{DOF}}}$ is the output influence matrix, and $\mathbf{H}_{\mathrm{c}}\in\mathbb{R}^{n_{\mathrm{y}}\times n_{\mathrm{d}}}$ is the input feedthrough matrix. A general case typically involves structural strain, displacement, and acceleration measurements, and the observation vector $\mathbf{y}(t)\in\mathbb{R}^{n_{\mathrm{y}}}$ can therefore be expressed by the sensor selection matrices as

$$\mathbf{y}(t)=\begin{bmatrix}\mathbf{S}_{\mathrm{str}} & \mathbf{0} & \mathbf{0}\\ \mathbf{0} & \mathbf{S}_{\mathrm{dis}} & \mathbf{0}\\ \mathbf{0} & \mathbf{0} & \mathbf{S}_{\mathrm{acc}}\end{bmatrix}\begin{bmatrix}\boldsymbol{\varepsilon}(t)\\ \mathbf{z}(t)\\ \ddot{\mathbf{z}}(t)\end{bmatrix} \tag{5}$$

Consequently, the matrices $\mathbf{C}_{\mathrm{c}}$ and $\mathbf{H}_{\mathrm{c}}$ become

$$\mathbf{C}_{\mathrm{c}}=\begin{bmatrix}\mathbf{S}_{\mathrm{str}}\mathbf{B}_{\mathrm{sd}} & \mathbf{0}\\ \mathbf{S}_{\mathrm{dis}} & \mathbf{0}\\ -\mathbf{S}_{\mathrm{acc}}\mathbf{M}^{-1}\mathbf{K} & -\mathbf{S}_{\mathrm{acc}}\mathbf{M}^{-1}\mathbf{C}\end{bmatrix},\quad \mathbf{H}_{\mathrm{c}}=\begin{bmatrix}\mathbf{0}\\ \mathbf{0}\\ \mathbf{S}_{\mathrm{acc}}\mathbf{M}^{-1}\mathbf{S}_{\mathrm{d}}\end{bmatrix} \tag{6}$$

The strain response $\boldsymbol{\varepsilon}(t)$ can be calculated as $\boldsymbol{\varepsilon}(t)=\mathbf{B}_{\mathrm{sd}}\mathbf{z}(t)$, where the transformation matrix $\mathbf{B}_{\mathrm{sd}}$ between the displacement and the strain is determined by the element type [13]. If only strain and displacement responses are measured (i.e., no accelerations), then the input feedthrough matrix $\mathbf{H}_{\mathrm{c}}$ becomes zero in the observation equation.

Given that structural responses are usually recorded in discrete time with a sampling time interval

Δt, the continuous state-space model in Eqs (2) and (3) are transferred into a discrete-time state-space model as

$$\mathbf{x}_{k+1} = \mathbf{A}_k \mathbf{x}_k + \mathbf{G}_k \mathbf{d}_k + \boldsymbol{\omega}_k \tag{7}$$

$$\mathbf{y}_k = \mathbf{C}_k \mathbf{x}_k + \mathbf{H}_k \mathbf{d}_k + \boldsymbol{\upsilon}_k \tag{8}$$

where $\mathbf{A}_k = \mathbf{e}^{\mathbf{A}_c \Delta t}$, $\mathbf{G}_k = \left[\mathbf{A}_k - \mathbf{I}\right]\mathbf{A}_c^{-1}\mathbf{G}_c$, $\mathbf{C}_k = \mathbf{C}_c$, and $\mathbf{H}_k = \mathbf{H}_c$. In the discretization process, the zero-order-hold assumption is adopted, which assumes a constant inter-sample behavior for the unknown input. $\boldsymbol{\omega}_k$ and $\boldsymbol{\upsilon}_k$ represent system error and measurement noise vectors, which are typically assumed as independent normally distributed white noise. Their covariance matrices are defined as $\mathrm{E}\left[\boldsymbol{\omega}_p \boldsymbol{\omega}_q^{\mathrm{T}}\right] = \mathbf{Q}\delta_{pq}$ and $\mathrm{E}\left[\boldsymbol{\upsilon}_p \boldsymbol{\upsilon}_q^{\mathrm{T}}\right] = \mathbf{R}\delta_{pq}$, where δ_{pq} is the Kronecker delta.

3. ULISE for structural response reconstruction

The two GDF algorithms provide the basis for most of the existing structural response reconstruction methods. Accelerometers are frequently adopted in SHM systems owing to their high sensitivity and relatively low noise. GDF-II, which has a direct feedthrough matrix [26], is commonly used in structural response reconstruction with unknown excitation input $\mathbf{d}_k$, and the input feedthrough matrix $\mathbf{H}_c \in \mathbb{R}^{n_y \times n_d}$ needs to have a full column rank n_d. A recursive three-step filter is defined in the GDF-II algorithm. The first step is the time update, where the state at time *k* is estimated using reconstructed values up to *k*-1. The unknown input is estimated in the second step. In the third step, the state estimation obtained in step one is updated using the measurement at time *k*.

To solve the problem of limited filter robustness under rank-deficient conditions, Hsieh [32] developed a filter that allowed the input estimate to be biased. In 2016, Yong et al. [31] then proposed a ULISE that overcomes the limitations of the traditional GDF-II filter by enabling input–state estimation without a full-rank feedthrough matrix. In the present study, the ULISE is applied to structural response reconstruction with unknown inputs. Unlike traditional response reconstruction methods that are only applicable to white-noise inputs, ULISE has no restrictions on the unknown inputs. Section 3.1 introduces the required system transformation, Section 3.2 presents the calculation procedure, and Section 3.3 discusses the normalization technique to solve the ill-conditioned problem.

3.1 System transformation

System transformation is conducted to decouple the system into parts with and without a full-rank direct feedthrough matrix, so that the ULISE can use the existing GDF algorithms for two individual conditions [25, 26].

Let $p_{\mathbf{H}_k} \triangleq \mathrm{rk}(\mathbf{H}_k)$. The system feedthrough matrix $\mathbf{H}_k$ can then be decoupled via singular value decomposition (SVD) as

$$\mathbf{H}_k = \mathbf{U}_k \begin{bmatrix} \mathbf{\Sigma}_k & \mathbf{0} \\ \mathbf{0} & \mathbf{0} \end{bmatrix} \mathbf{V}_k^{\mathrm{T}} = \begin{bmatrix} \mathbf{U}_{1,k} & \mathbf{U}_{2,k} \end{bmatrix} \begin{bmatrix} \mathbf{\Sigma}_k & \mathbf{0} \\ \mathbf{0} & \mathbf{0} \end{bmatrix} \begin{bmatrix} \mathbf{V}_{1,k}^{\mathrm{T}} \\ \mathbf{V}_{2,k}^{\mathrm{T}} \end{bmatrix} \tag{9}$$

where $\mathbf{U}_{1,k} \in \mathbb{R}^{n_{\mathrm{y}} \times p_{\mathbf{H}_k}}$, $\mathbf{U}_{2,k} \in \mathbb{R}^{n_{\mathrm{y}} \times (n_{\mathrm{y}} - p_{\mathbf{H}_k})}$, $\mathbf{V}_{1,k} \in \mathbb{R}^{n_{\mathrm{d}} \times p_{\mathbf{H}_k}}$, $\mathbf{V}_{2,k} \in \mathbb{R}^{n_{\mathrm{d}} \times (n_{\mathrm{d}} - p_{\mathbf{H}_k})}$, $\mathbf{U}_k \triangleq \begin{bmatrix} \mathbf{U}_{1,k} & \mathbf{U}_{2,k} \end{bmatrix}$, and $\mathbf{V}_k \triangleq \begin{bmatrix} \mathbf{V}_{1,k} & \mathbf{V}_{2,k} \end{bmatrix}$ are unitary matrices, and $\mathbf{\Sigma}_k \in \mathbb{R}^{p_{\mathbf{H}_k} \times p_{\mathbf{H}_k}}$ is a full-rank diagonal matrix. The roundoff error may affect the SVD calculation. In practice, each element of $\mathbf{\Sigma}_k$ is checked against a small tolerance instead of zero to ensure that the roundoff error does not affect the rank number $p_{\mathbf{H}_k}$ of the matrix $\mathbf{\Sigma}_k$.

As recommended by Cheng et al. [33], two orthogonal components of the unknown input are defined as Eq. (10), where $\mathbf{d}_{1,k}$ corresponds to the full-rank component of the system. Given that $\mathbf{V}_k \triangleq \begin{bmatrix} \mathbf{V}_{1,k} & \mathbf{V}_{2,k} \end{bmatrix}$ is a unitary matrix, the arbitrary unknown input $\mathbf{d}_k$ can be calculated as Eq. (11).

$$\mathbf{d}_{1,k} = \mathbf{V}_{1,k}^{\mathrm{T}} \mathbf{d}_k, \quad \mathbf{d}_{2,k} = \mathbf{V}_{2,k}^{\mathrm{T}} \mathbf{d}_k \tag{10}$$

$$\mathbf{d}_k = \mathbf{V}_{1,k} \mathbf{d}_{1,k} + \mathbf{V}_{2,k} \mathbf{d}_{2,k} \tag{11}$$

The state-space equation for a system under unknown inputs in discrete time can therefore be expressed as

$$\mathbf{x}_{k+1} = \mathbf{A}_k \mathbf{x}_k + \mathbf{G}_{1,k} \mathbf{d}_{1,k} + \mathbf{G}_{2,k} \mathbf{d}_{2,k} + \boldsymbol{\omega}_k \tag{12}$$

$$\mathbf{y}_k = \mathbf{C}_k \mathbf{x}_k + \mathbf{H}_{1,k} \mathbf{d}_{1,k} + \boldsymbol{\upsilon}_k \tag{13}$$

where $\mathbf{G}_{1,k} \triangleq \mathbf{G}_k \mathbf{V}_{1,k}$, $\mathbf{G}_{2,k} \triangleq \mathbf{G}_k \mathbf{V}_{2,k}$, and $\mathbf{H}_{1,k} \triangleq \mathbf{H}_k \mathbf{V}_{1,k} = \mathbf{U}_{1,k} \mathbf{\Sigma}_k$.

The observation vector $\mathbf{y}_k$ is then decoupled using a nonsingular transformation $\mathbf{T}_k$, and the output can be represented by $\mathbf{z}_{1,k}$ and $\mathbf{z}_{2,k}$.

$$\mathbf{T}_k = \begin{bmatrix} \mathbf{T}_{1,k} \\ \mathbf{T}_{2,k} \end{bmatrix} \tag{14}$$

$$\mathbf{T}_{1,k} = \mathbf{U}_{1,k} - \left[\mathbf{U}_{1,k}^{\mathrm{T}} \mathbf{R}_k \mathbf{U}_{2,k} \left(\mathbf{U}_{2,k}^{\mathrm{T}} \mathbf{R}_k \mathbf{U}_{2,k} \right)^{-1} \mathbf{U}_{2,k}^{\mathrm{T}} \right]^{\mathrm{T}} \tag{15}$$

$$\mathbf{T}_{2,k} = \mathbf{U}_{2,k} \tag{16}$$

$$\mathbf{z}_{1,k} = \mathbf{T}_{1,k} \mathbf{y}_k = \mathbf{C}_{1,k} \mathbf{x}_k + \mathbf{\Sigma}_k \mathbf{d}_{1,k} + \boldsymbol{\upsilon}_{1,k} \tag{17}$$

$$\mathbf{z}_{2,k} = \mathbf{T}_{2,k} \mathbf{y}_k = \mathbf{C}_{2,k} \mathbf{x}_k + \boldsymbol{\upsilon}_{2,k} \tag{18}$$

where $\mathbf{C}_{1,k} \triangleq \mathbf{T}_{1,k} \mathbf{C}_k$, and $\mathbf{C}_{2,k} \triangleq \mathbf{T}_{2,k} \mathbf{C}_k = \mathbf{U}_{2,k}^{\mathrm{T}} \mathbf{C}_k$.

Similarly, the covariance matrix for measurement noise $\mathbf{R}_k \in \mathbb{R}^{n_y \times n_y}$ can also be decoupled as

$$\mathbf{R}_{1,k} \triangleq \mathbf{T}_{1,k} \mathbf{R}_k \mathbf{T}_{1,k}^{\mathrm{T}} \tag{19}$$

$$\mathbf{R}_{2,k} \triangleq \mathbf{T}_{2,k} \mathbf{R}_k \mathbf{T}_{2,k}^{\mathrm{T}} = \mathbf{U}_{2,k}^{\mathrm{T}} \mathbf{R}_k \mathbf{U}_{2,k} \tag{20}$$

3.2 ULISE algorithm

Similar to the GDF-II algorithm, the ULISE adopts a recursive three-step design. Given observations at time *k*, the unknown input at the last time step *k*-1 is first estimated using the current measurement. The state estimation is based on the minimum-variance-unbiased optimization. Then, the state estimate propagates from time *k*-1 to time *k* based on system dynamics and input estimation from the first step Finally, the state estimation is updated using the observations at time *k* in the measurement update step. The three steps of the recursive filter are presented as follows:

Unknown input estimation

$$\hat{\mathbf{d}}_{1,k} = \mathbf{M}_{1,k} \left(\mathbf{z}_{1,k} - \mathbf{C}_{1,k} \hat{\mathbf{x}}_{k|k} \right) \tag{21}$$

$$\hat{\mathbf{d}}_{2,k-1} = \mathbf{M}_{2,k} \left(\mathbf{z}_{2,k} - \mathbf{C}_{2,k} \hat{\mathbf{x}}_{k|k-1} \right) \tag{22}$$

$$\hat{\mathbf{d}}_{k-1} = \mathbf{V}_{1,k-1} \hat{\mathbf{d}}_{1,k-1} + \mathbf{V}_{2,k-1} \hat{\mathbf{d}}_{2,k-1} \tag{23}$$

Time update

$$\hat{\mathbf{x}}_{k|k-1} = \mathbf{A}_{k-1} \hat{\mathbf{x}}_{k-1|k-1} + \mathbf{G}_{1,k-1} \hat{\mathbf{d}}_{1,k-1} \tag{24}$$

$$\hat{\mathbf{x}}_{k|k}^{*} = \hat{\mathbf{x}}_{k|k-1} + \mathbf{G}_{2,k-1} \hat{\mathbf{d}}_{2,k-1} \tag{25}$$

Measurement update

$$\hat{\mathbf{x}}_{k|k} = \hat{\mathbf{x}}_{k|k}^{*} + \mathbf{L}_k \left(\mathbf{y}_k - \mathbf{C}_k \hat{\mathbf{x}}_{k|k}^{*} \right) = \hat{\mathbf{x}}_{k|k}^{*} + \tilde{\mathbf{L}}_k \left(\mathbf{z}_{2,k} - \mathbf{C}_{2,k} \hat{\mathbf{x}}_{k|k}^{*} \right) \tag{26}$$

The iteration steps for the ULISE are summarized in **Algorithm 1.** $\hat{\mathbf{x}}_{k|k}$ and $\hat{\mathbf{d}}_{k-1}$ represent the minimum-variance unbiased optimal estimates of the state vector at time *k* and the unknown input at time *k*-1, respectively. Estimation error covariance matrices for the state vector and input are defined as

$$\mathbf{P}_{k|k}^{\mathbf{x}} = \mathrm{E}\left[\left(\mathbf{x}_k - \hat{\mathbf{x}}_{k|k} \right) \left(\mathbf{x}_k - \hat{\mathbf{x}}_{k|k} \right)^{\mathrm{T}} \right] \tag{27}$$

$$\mathbf{P}_{k-1}^{\mathbf{d}} = \mathrm{E}\left[\left(\mathbf{d}_{k-1} - \hat{\mathbf{d}}_{k-1} \right) \left(\mathbf{d}_{k-1} - \hat{\mathbf{d}}_{k-1} \right)^{\mathrm{T}} \right] \tag{28}$$

$\mathbf{M}_{1,k}$, $\mathbf{M}_{2,k}$, and $\mathbf{L}_k$ are filter gain matrices selected to minimize the state and input error covariances.

The unknown input component $\hat{\mathbf{d}}_{1,k}$ is estimated in the current step, while the component $\hat{\mathbf{d}}_{2,k}$ is estimated with a one-step delay. Therefore, the ULISE filter implements a two-step estimation for input $\mathbf{d}_k$ under rank-deficient feedthrough matrix conditions. However, under full-rank feedthrough matrix $\mathbf{H}_k$ conditions, $\mathbf{U}_{2,k}$ and $\mathbf{V}_{2,k}$ become zero in Eq. (9), and consequently, $\hat{\mathbf{d}}_{2,k}$ estimation is unnecessary. The input $\mathbf{d}_k$ is estimated in one step (the current step), which is essentially equivalent to the GDF-II filter.

3.3 Normalization

Multi-type sensor data fusion processes commonly feature ill-conditioned matrices [13]. Measured accelerations, velocities, displacements, and strains are usually in different orders of magnitude. The inversion or pseudoinversion of the matrix with a considerable condition number often leads to large computation errors. Therefore, normalization is first conducted to ensure the numerical stability of the ULISE during the fusion of different sensor signal types. A weighting matrix $\mathbf{W}_k$, calculated as the inverse of the square root of the predefined measurement noise covariance matrix $\mathbf{R}_k$, is adopted to scale the estimated responses for different sensor types:

$$\mathbf{W}_k = \mathbf{R}_k^{-1/2} \tag{29}$$

The weighting matrix $\mathbf{W}_k$ is determined before the ULISE iterations and is assumed to be constant during the calculation.

The normalized output influence matrix $\bar{\mathbf{C}}_k$, feedthrough matrix $\bar{\mathbf{H}}_k$, and measurement noise

covariance matrix $\bar{\mathbf{R}}_k$ are computed as

$$\bar{\mathbf{C}}_k = \mathbf{W}_k \mathbf{C}_k, \quad \bar{\mathbf{H}}_k = \mathbf{W}_k \mathbf{H}_k, \quad \bar{\mathbf{R}}_k = \mathbf{W}_k^2 \mathbf{R}_k \tag{30}$$

The observation vector $\mathbf{y}_k$ is normalized as

$$\bar{\mathbf{y}}_k = \mathbf{W}_k \mathbf{y}_k \tag{31}$$

The bar symbol in Eqs (30) and (31) and Algorithm 1 corresponds to normalized vectors or matrices. After normalization, the ULISE can stably fuse different signals.

Algorithm 1

ULISE algorithm with sensor data normalization

Calculation steps
1. Define the state-space model $\mathbf{x}_{k+1} = \mathbf{A}_k \mathbf{x}_k + \mathbf{G}_k \mathbf{d}_k + \boldsymbol{\omega}_k$ $\mathbf{y}_k = \mathbf{C}_k \mathbf{x}_k + \mathbf{H}_k \mathbf{d}_k + \boldsymbol{\upsilon}_k$
2. Normalization $\mathbf{W}_k = \mathbf{R}_k^{-1/2}$ $\bar{\mathbf{C}}_k = \mathbf{W}_k \mathbf{C}_k$ $\bar{\mathbf{H}}_k = \mathbf{W}_k \mathbf{H}_k$ $\bar{\mathbf{R}}_k = \mathbf{W}_k^2 \mathbf{R}_k$ $\bar{\mathbf{y}}_k = \mathbf{W}_k \mathbf{y}_k$ $\mathbf{x}_{k+1} = \mathbf{A}_k \mathbf{x}_k + \mathbf{G}_k \mathbf{d}_k + \boldsymbol{\omega}_k$ $\bar{\mathbf{y}}_k = \bar{\mathbf{C}}_k \mathbf{x}_k + \bar{\mathbf{H}}_k \mathbf{d}_k + \bar{\boldsymbol{\upsilon}}_k$
3. System transformation and initialization
4. Iteration steps for k = 1:N
● Input estimation: $\hat{\mathbf{d}}_{2,k-1}$ and $\hat{\mathbf{d}}_{k-1}$

$$\tilde{\mathbf{P}}_k = \hat{\mathbf{A}}_{k-1}\mathbf{P}^{\mathbf{x}}_{k-1|k-1}\hat{\mathbf{A}}^{\mathrm{T}}_{k-1} + \hat{\mathbf{Q}}_{k-1}$$

$$\tilde{\mathbf{R}}_{2,k} = \bar{\mathbf{C}}_{2,k}\tilde{\mathbf{P}}_k\bar{\mathbf{C}}^{\mathrm{T}}_{2,k} + \bar{\mathbf{R}}_{2,k}$$

$$\mathbf{P}^{\mathbf{d}}_{2,k-1} = \left(\mathbf{G}^{\mathrm{T}}_{2,k-1}\bar{\mathbf{C}}^{\mathrm{T}}_{2,k}\tilde{\mathbf{R}}^{-1}_{2,k}\bar{\mathbf{C}}_{2,k}\mathbf{G}_{2,k-1}\right)^{-1}$$

$$\mathbf{M}_{2,k} = \mathbf{P}^{\mathbf{d}}_{2,k-1}\mathbf{G}^{\mathrm{T}}_{2,k-1}\bar{\mathbf{C}}^{\mathrm{T}}_{2,k}\tilde{\mathbf{R}}^{-1}_{2,k}$$

$$\hat{\mathbf{x}}_{k|k-1} = \mathbf{A}_{k-1}\hat{\mathbf{x}}_{k-1|k-1} + \mathbf{G}_{1,k-1}\hat{\mathbf{d}}_{1,k-1}$$

$$\hat{\mathbf{d}}_{2,k-1} = \mathbf{M}_{2,k}\left(\bar{\mathbf{z}}_{2,k} - \bar{\mathbf{C}}_{2,k}\hat{\mathbf{x}}_{k|k-1}\right)$$

$$\hat{\mathbf{d}}_{k-1} = \mathbf{V}_{1,k-1}\hat{\mathbf{d}}_{1,k-1} + \mathbf{V}_{2,k-1}\hat{\mathbf{d}}_{2,k-1}$$

$$\mathbf{P}^{\mathbf{d}}_{12,k-1} = \mathbf{M}_{1,k-1}\bar{\mathbf{C}}_{1,k-1}\mathbf{P}^{\mathbf{x}}_{k-1|k-1}\mathbf{A}^{\mathrm{T}}_{k-1}\bar{\mathbf{C}}^{\mathrm{T}}_{2,k}\mathbf{M}^{\mathrm{T}}_{2,k} - \mathbf{P}^{\mathbf{d}}_{1,k-1}\mathbf{G}^{\mathrm{T}}_{1,k-1}\bar{\mathbf{C}}^{\mathrm{T}}_{2,k}\mathbf{M}^{\mathrm{T}}_{2,k}$$

$$\mathbf{P}^{\mathbf{d}}_{k-1} = \mathbf{V}_{k-1}\begin{bmatrix}\mathbf{P}^{\mathbf{d}}_{1,k-1} & \mathbf{P}^{\mathbf{d}}_{12,k-1}\\ \mathbf{P}^{\mathbf{d}\ \mathrm{T}}_{12,k-1} & \mathbf{P}^{\mathbf{d}}_{2,k-1}\end{bmatrix}\mathbf{V}^{\mathrm{T}}_{k-1}$$

- The time update of the state

$$\hat{\mathbf{x}}^{*}_{k|k} = \hat{\mathbf{x}}_{k|k-1} + \mathbf{G}_{2,k-1}\hat{\mathbf{d}}_{2,k-1}$$

$$\mathbf{P}^{*\mathbf{x}}_{k|k} = \mathbf{G}_{2,k-1}\mathbf{M}_{2,k}\bar{\mathbf{R}}_{2,k}\mathbf{M}^{\mathrm{T}}_{2,k}\mathbf{G}^{\mathrm{T}}_{2,k} + \left(\mathbf{I} - \mathbf{G}_{2,k-1}\mathbf{M}_{2,k}\bar{\mathbf{C}}_{2,k}\right)\tilde{\mathbf{P}}_k\left(\mathbf{I} - \mathbf{G}_{2,k-1}\mathbf{M}_{2,k}\bar{\mathbf{C}}_{2,k}\right)^{\mathrm{T}}$$

$$\tilde{\mathbf{R}}^{*}_{k} = \bar{\mathbf{C}}_k\mathbf{P}^{*\mathbf{x}}_{k|k}\bar{\mathbf{C}}^{\mathrm{T}}_k + \bar{\mathbf{R}}_k - \bar{\mathbf{C}}_k\mathbf{G}_{2,k-1}\mathbf{M}_{2,k}\mathbf{U}^{\mathrm{T}}_{2,k}\bar{\mathbf{R}}_k - \bar{\mathbf{R}}_k\mathbf{U}_{2,k}\mathbf{M}^{\mathrm{T}}_{2,k}\mathbf{G}^{\mathrm{T}}_{2,k-1}\bar{\mathbf{C}}^{\mathrm{T}}_k$$

- The measurement update of the state

$$\mathbf{K}_k = \mathbf{P}^{*\mathbf{x}}_{k|k}\bar{\mathbf{C}}^{\mathrm{T}}_k - \mathbf{G}_{2,k-1}\mathbf{M}_{2,k}\mathbf{U}^{\mathrm{T}}_{2,k}\bar{\mathbf{R}}_k$$

$$\mathbf{M}^{*}_{1,k} = \mathbf{\Sigma}^{-1}_k\left(\mathbf{U}^{T}_{1,k}\left(\tilde{\mathbf{R}}^{*}_k\right)^{\dagger}\mathbf{U}_{1,k}\right)^{-1}\mathbf{U}^{T}_{1,k}\left(\tilde{\mathbf{R}}^{*}_k\right)^{\dagger}$$

$$\mathbf{L}_k = \mathbf{K}_k\left(\mathbf{I} - \mathbf{U}_{1,k}\mathbf{\Sigma}_k\mathbf{M}^{*}_{1,k}\right)^{\mathrm{T}}\left(\tilde{\mathbf{R}}^{*}_k\right)^{\dagger}$$

$$\hat{\mathbf{x}}_{k|k} = \hat{\mathbf{x}}^{*}_{k|k} + \mathbf{L}_k\left(\bar{\mathbf{y}}_k - \bar{\mathbf{C}}_k\hat{\mathbf{x}}^{*}_{k|k}\right)$$

$$\mathbf{P}^{\mathbf{x}}_{k|k} = \left(\mathbf{I} - \mathbf{L}_k\bar{\mathbf{C}}_k\right)\mathbf{G}_{2,k-1}\mathbf{M}_{2,k}\mathbf{U}^{\mathrm{T}}_{2,k}\bar{\mathbf{R}}_k\mathbf{L}^{\mathrm{T}}_k + \mathbf{L}_k\bar{\mathbf{R}}_k\mathbf{U}_{2,k}\mathbf{M}^{\mathrm{T}}_{2,k}\mathbf{G}^{\mathrm{T}}_{2,k-1}\left(\mathbf{I} - \mathbf{L}_k\bar{\mathbf{C}}_k\right)^{\mathrm{T}}$$

$$+\left(\mathbf{I} - \mathbf{L}_k\bar{\mathbf{C}}_k\right)\mathbf{P}^{*\mathbf{x}}_{k|k}\left(\mathbf{I} - \mathbf{L}_k\bar{\mathbf{C}}_k\right)^{\mathrm{T}} + \mathbf{L}_k\bar{\mathbf{R}}_k\mathbf{L}^{\mathrm{T}}_k$$

- Input estimation: $\hat{\mathbf{d}}_{1,k}$

$$\tilde{\mathbf{R}}_{1,k} = \bar{\mathbf{C}}_{1,k}\mathbf{P}^{\mathbf{x}}_{k|k}\bar{\mathbf{C}}^{\mathrm{T}}_{1,k} + \bar{\mathbf{R}}_{1,k}$$

$$\mathbf{M}_{1,k} = \mathbf{\Sigma}^{-1}_k$$

$$\mathbf{P}^{\mathbf{d}}_{1,k} = \mathbf{M}_{1,k}\tilde{\mathbf{R}}_{1,k}\mathbf{M}_{1,k}$$

$$\hat{\mathbf{d}}_{1,k} = \mathbf{M}_{1,k}\left(\bar{\mathbf{z}}_{1,k} - \bar{\mathbf{C}}_{1,k}\hat{\mathbf{x}}_{k|k}\right)$$

$$\hat{\mathbf{A}}_k = \mathbf{A}_k - \mathbf{G}_{1,k}\mathbf{M}_{1,k}\bar{\mathbf{C}}_{1,k}$$

$$\hat{\mathbf{Q}}_k = \mathbf{G}_{1,k}\mathbf{M}_{1,k}\mathbf{R}_{1,k}\mathbf{M}^{\mathrm{T}}_{1,k}\mathbf{G}^{\mathrm{T}}_{1,k} + \mathbf{Q}_k$$

end

Note: † refers to the Moore–Penrose pseudoinverse

^ refers to the estimated vectors

¯ refers to the normalized matrices

4. Numerical study

4.1 Eight-story shear frame model

Numerical simulations of an eight-story shear frame are conducted to evaluate the applicability and performance of the proposed ULISE-based response reconstruction algorithm. The structure was first presented by Callafon et al. [34], and later, Azam et al. [35] used this frame in state estimation by a dual KF. The story mass is 625,000 kg, and the inter-story lateral stiffness is assumed to be 10^6 kN/m. The damping ratios for all modes are assumed to be 2%. Different from Refs. [34,35], which used acceleration responses, this study uses the measured acceleration and strain data for response reconstruction. The strain responses are calculated according to $\boldsymbol{\varepsilon}(t) = \mathbf{B}_{\text{sd}}\mathbf{z}(t)$, where $\mathbf{B}_{\text{sd}}$ is the transformation matrix calculated from the column dimensions, and $\mathbf{z}(t)$ is the displacement response. Because the dimension information was not provided in [34, 35], this study assumes that the story height is 4 m, and the section height of the column is 0.5 m. **Fig. 1** shows the overview of the shear frame system. The undamped natural frequencies of this frame are presented in **Table 1**.

Table 1

Undamped natural frequencies of the structure

Mode No.	1	2	3	4	5	6	7	8
Frequency (Hz)	1.17	3.48	5.67	7.67	9.41	10.83	11.87	12.52

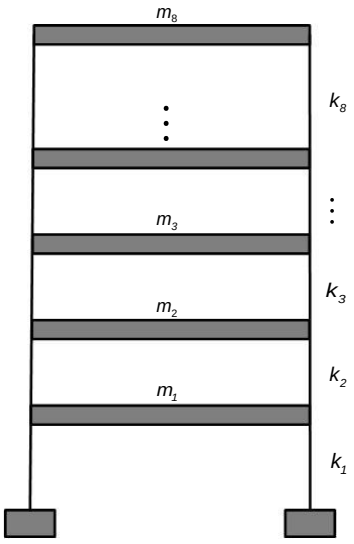

Fig. 1. Overview of an 8DOF shear frame.

4.2 Simulation results

Without loss of generality, the filter performances are verified using strain gauges and accelerometers at different locations. The locations of input loads and accelerometers directly correspond to DOFs of the frame. Strain gauges are installed on the columns to measure the bending strain, and they do not directly measure any specific DOFs. Instead, bending strain is proportional to inter-story drifts (i.e., the relative displacements between two adjacent DOFs). Eight cases are simulated and compared to test the filter robustness under various conditions. The eight cases consider different influencing factors, including different input types (Case 1 vs. Case 2, Case 5 vs. Case 6), different sensor numbers (Case 1 vs. Case 3, Case 5 vs. Case 7), and different sensor noise levels (Case 1 vs. Case 4, Case 5 vs. Case 8) (see **Table 2**). Case 9 presents non-collocated measurements, in which some input DOFs are monitored by neither accelerometers nor strain gauges. The feedthrough matrix $\mathbf{H}_k$ is full rank in Cases 1 – 4, while $\mathbf{H}_k$ is rank-deficient in Cases 5 - 9. Random and harmonic inputs are typical input types in the field of structural dynamics and are therefore adopted in the simulations. In 2014, Maes et al. [30] presented a detailed guideline for sensor network design. This section elucidates the filter performance in Cases 1-8. The performance with non-collocated measurements will be evaluated in Section 4.3.

Table 2

Simulation cases

Case No.	Input locations (DOF)	Input type	Sensor locations		Measurement noise level
			Accelerometer (DOF)	Strain (Story No.)	
1	2 5 8	Random	2 5 8	2 5 8	2%
2	2 5 8	Harmonic	2 5 8	2 5 8	2%
3	2 5 8	Random	2 5 8	2 4 5 6 8	2%
4	2 5 8	Random	2 5 8	2 5 8	10%
5	2 5 8	Random	8	2 5 8	2%
6	2 5 8	Harmonic	8	2 5 8	2%
7	2 5 8	Random	8	2 4 5 6 8	2%
8	2 5 8	Random	8	2 5 8	10%
9	2 5 8	Random	8	1 3 6	2%

The traditional GDF-II algorithm [26] frequently applied in response reconstruction is only applicable to cases in which the direct feedthrough matrix $\mathbf{H}_k$ is full rank, that is, the number of accelerometers is equal to or exceeds the number of unknown inputs. Therefore, the GDF-II is only applicable to Cases 1 – 4 in **Table 2**, wherein the accelerations are observed at all the DOFs with unknown inputs so that the full rank requirement is satisfied. The GDF-I algorithm [25] based on only displacement (or strain) measurement is prone to losing high-frequency contents and is therefore not a common choice in structural response reconstruction. By contrast, the ULISE algorithm does not require a full rank condition of the feedthrough matrix and is applicable to all the cases, including the rank deficient Cases 5 – 8 in **Table 2**.

As shown in **Table 2**, two types of inputs are defined. The detailed information on these inputs is presented in **Table 3**. The frequency ranges of the random inputs are 0.01–1 Hz, 0.1–10 Hz, and 0.5–15 Hz for the three DOFs. They are designed to cover the natural frequencies of the shear frame. The selection of noise levels may influence filter performance. The measurement noise covariance matrix $\mathbf{R}_k$ represents the sensor noise level. In this study, noise covariance is assumed constant for each type of sensors and independent of the sensor locations and measured signals. Two measurement noise levels are predefined, whose standard deviations are estimated at approximately 2% and 10% of the responses' standard deviations. Subsequently, filter stability under different noise levels can be tested. In all eight cases, the structural model deployed in the algorithm is assumed to be reasonably accurate; thus, the system noise term $\mathbf{Q}$ is set to a small value, that is, $\mathbf{Q}_k = 10^{-20} \times \mathbf{I}$. The same value was also adopted in [35].

The normalized root-mean-square error (NRMSE) is frequently used as the filter performance indicator in response reconstruction. For the estimated response $\hat{x}_k$ and its theoretical response x_k, the root-mean-square error (RMSE) is first calculated using Eq. (32); then, the NRMSE is calculated using Eq. (33). A smaller NRMSE corresponds to better filter performance.

Table 3

Detailed information on the applied inputs

Input type	Input DOF		
	2	5	8

	Amplitude (N)	Frequency (Hz)	Amplitude (N)	Frequency (Hz)	Amplitude (N)	Frequency (Hz)
Random	3×10^5	0.01–1	3×10^5	0.1–10	3×10^5	0.5–15
Harmonic	8×10^5	1	8×10^5	12	8×10^5	0.01 and 0.1

$$RMSE = \sqrt{\frac{\sum_{k=1}^{n}\left(x_k - \hat{x}_k\right)^2}{n}} \tag{32}$$

$$NRMSE = \frac{RMSE}{x_{\max} - x_{\min}} \tag{33}$$

Fig. 2 shows the bar plot of NRMSEs estimated by the proposed ULISE algorithm for the state vector (displacement) in Cases 5–8. The eight ratios in each case correspond to the relative reconstruction errors for the displacements from the first to eighth floors. The velocity and strain reconstruction errors are qualitatively similar to the displacements and are therefore omitted for conciseness. The detailed NRMSE data for the displacement estimation are summarized in **Table 4**. **Fig. 3** presents the reconstruction NRMSE for the three unknown excitations in the rank-deficient scenarios. Notably, the GDF-II filter is not directly applicable to Cases 5–8 because the rank deficient feedthrough matrix (i.e., not all of the DOFs with input are monitored by accelerometers). If we ignore the inputs at the DOFs without any accelerometers (i.e., the corresponding inputs are assumed to be zero in the filter), the GDF-II filter can be proceeded but associated with inevitably large reconstruction errors. Therefore, the GDF-II algorithm is not presented for Cases 5-8 in Table 5.

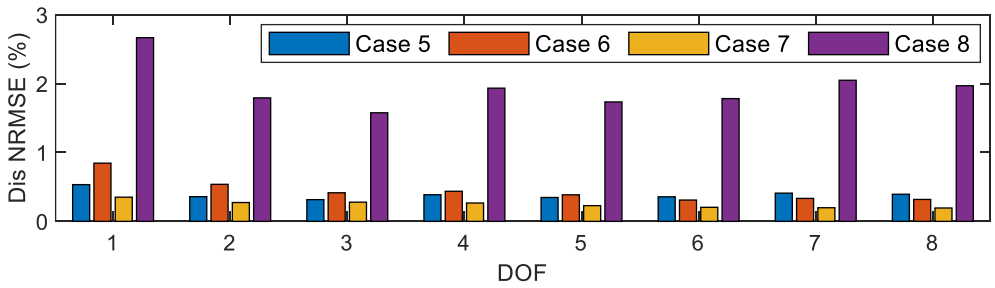

Fig. 2. Bar plot of the displacement NRMSE (%) estimated by ULISE.

As illustrated in **Table 2**, the first four cases are under full-rank conditions. Cases 1–4 consider different input types (Case 1 vs. Case 2), sensor numbers (Case 1 vs. Case 3), and sensor noise levels (Case 1 vs. Case 4). For the first four cases, the ULISE and GDF-II exhibit the same performance for both state estimation and input reconstruction (**Tables 4** and **5**). This substantiates the aforementioned conclusion that the proposed ULISE-based algorithm is identical to the traditional GDF-II method under full-rank conditions. The comparison between Cases 1 and 3 indicates that increasing the number of sensors (two more strain gauges in Case 3) can improve the reconstruction accuracy in the responses and inputs. The comparison between Cases 1 and 4 indicates that a higher measurement noise level leads to significant degradation in filter performance.

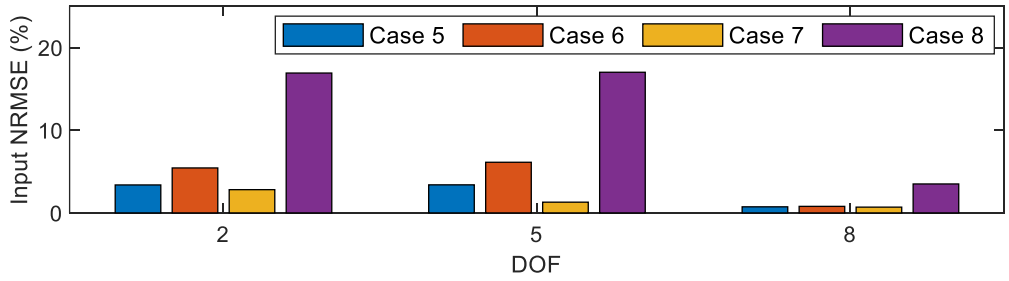

Fig. 3. Bar plot of the input NRMSE (%) estimated by ULISE.

Table 4

NRMSEs for displacement reconstruction

Case	Algorithm	NRMSE (%)							
		DOF1	DOF2	DOF3	DOF4	DOF5	DOF6	DOF7	DOF8
1	ULISE	0.2405	0.2515	0.2213	0.2169	0.2137	0.1990	0.1973	0.2008
	GDF-II	0.2405	0.2515	0.2213	0.2169	0.2137	0.1990	0.1973	0.2008
2	ULISE	0.2993	0.2881	0.2253	0.2087	0.2000	0.1926	0.1955	0.1968
	GDF-II	0.2993	0.2881	0.2253	0.2087	0.2000	0.1926	0.1955	0.1968
3	ULISE	0.2385	0.2487	0.2194	0.2084	0.1982	0.1824	0.1769	0.1788
	GDF-II	0.2385	0.2487	0.2194	0.2084	0.1982	0.1824	0.1769	0.1788
4	ULISE	1.2026	1.2576	1.1065	1.0843	1.0687	0.9948	0.9867	1.0038
	GDF-II	1.2026	1.2576	1.1065	1.0843	1.0687	0.9948	0.9867	1.0038
5	ULISE	0.5332	0.3585	0.3152	0.3867	0.3466	0.3564	0.4096	0.3936
	GDF-II	N/A	N/A	N/A	N/A	N/A	N/A	N/A	N/A
6	ULISE	0.8449	0.5375	0.4148	0.4367	0.3853	0.3093	0.3331	0.3183
	GDF-II	N/A	N/A	N/A	N/A	N/A	N/A	N/A	N/A

7	ULISE	0.3510	0.2734	0.2785	0.2664	0.2283	0.2039	0.1977	0.1940
	GDF-II	N/A	N/A	N/A	N/A	N/A	N/A	N/A	N/A
8	ULISE	2.6661	1.7924	1.5759	1.9333	1.7332	1.7819	2.0479	1.9681
	GDF-II	N/A	N/A	N/A	N/A	N/A	N/A	N/A	N/A

Under rank-deficient direct feedthrough matrix conditions, that is, the number of accelerometers is less than the number of unknown inputs, the ULISE outperforms GDF-II. GDF-II is no longer applicable in these cases (Cases 5–8), while the proposed ULISE algorithm can still reconstruct the states and inputs in these cases with relatively high accuracy. Cases 5–8 are designed to examine the filter robustness under rank-deficient conditions in different scenarios, including different input types (Case 5 vs. Case 6), sensor numbers (Case 5 vs. Case 7), and sensor noise levels (Case 5 vs. Case 8). Generally, Cases 5–8 exhibit greater estimation errors than Cases 1–4 because fewer accelerometers are installed in Cases 5–8.

For most of the scenarios (i.e., Cases 5–7), ULISE exhibits satisfactory performance in terms of the input estimation NRMSE (**Fig. 3**). Generally, the estimation errors under input locations without accelerometers (DOF2 and DOF5) are greater than that at the DOF with an accelerometer (i.e., DOF8). In Case 8, the input reconstruction features relatively large errors because of the relatively high measurement noise (10% of the standard deviation of structural responses). However, the ULISE still provides reasonably good state reconstruction accuracy in Case 8 (**Table 4**).

Table 5

NRMSEs for unknown input reconstruction

Case	Algorithm	NRMSE (%)		
		DOF2	DOF5	DOF8
1	ULISE	1.170	3.472	0.749
	GDF-II	1.170	3.472	0.749
2	ULISE	1.780	3.180	0.730
	GDF-II	1.780	3.180	0.730
3	ULISE	1.051	2.949	0.672
	GDF-II	1.051	2.949	0.672
4	ULISE	5.026	5.500	3.300
	GDF-II	5.026	5.500	3.300
5	ULISE	3.382	3.395	0.737
	GDF-II	N/A	N/A	N/A
6	ULISE	5.438	6.125	0.791

	GDF-II	N/A	N/A	N/A
7	ULISE	2.812	1.298	0.698
	GDF-II	N/A	N/A	N/A
8	ULISE	16.917	17.012	3.501
	GDF-II	N/A	N/A	N/A

The input reconstruction performances of ULISE in Case 5 with a rank-deficient condition are depicted in **Fig. 4**. Only inputs for 15–20 s are plotted to elucidate the comparison. The ULISE algorithm can reconstruct the unknown inputs even in the absence of an accelerometer. At DOF2 and DOF5, the NRMSEs are 3.382% and 3.395%, respectively. The presence of an accelerometer at DOF8 considerably reduces the input reconstruction error, and the corresponding NRMSE is only 0.737%, which is around 22% of those at DOF2 and DOF5 without accelerometers. Although the installation of accelerometers at the input DOF can improve the reconstruction performance, the proposed ULISE algorithm can still provide reasonably satisfactory results when applied to the cases with rank-deficient feedthrough matrices.

The responses at DOF7 obtained in Case 5 are presented in **Fig. 5** to examine the state estimation effectiveness of the proposed ULISE. Neither the acceleration nor the strain is recorded at DOF7, and the responses are obtained from response reconstruction. The ULISE-estimated time histories for the acceleration, velocity, displacement, and strain and their real counterparts are compared in **Fig. 5**. The ULISE provides reasonably accurate estimations of the state vectors, substantiated by the NRMSE values in **Table 4**. The NRMSE values for displacement are all within 0.55% in Case 5. These results demonstrate the effectiveness and accuracy of the proposed ULISE algorithm.

(a)

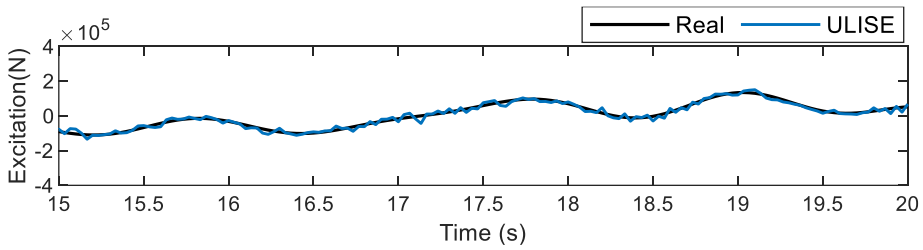

(b)

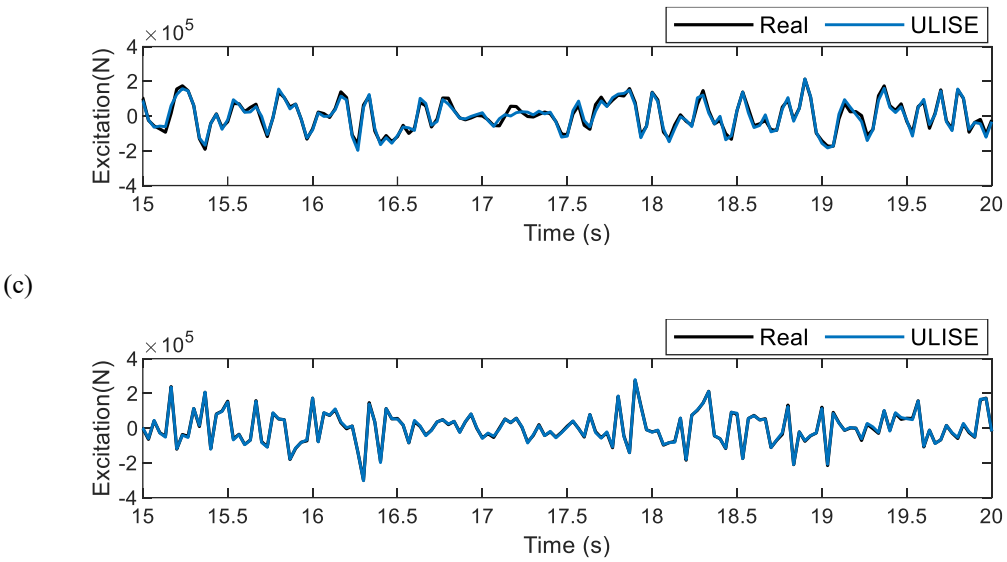

Fig. 4. ULISE-estimated time histories of excitations in Case 5 at (a) DOF2, (b) DOF5, (c) and DOF8.

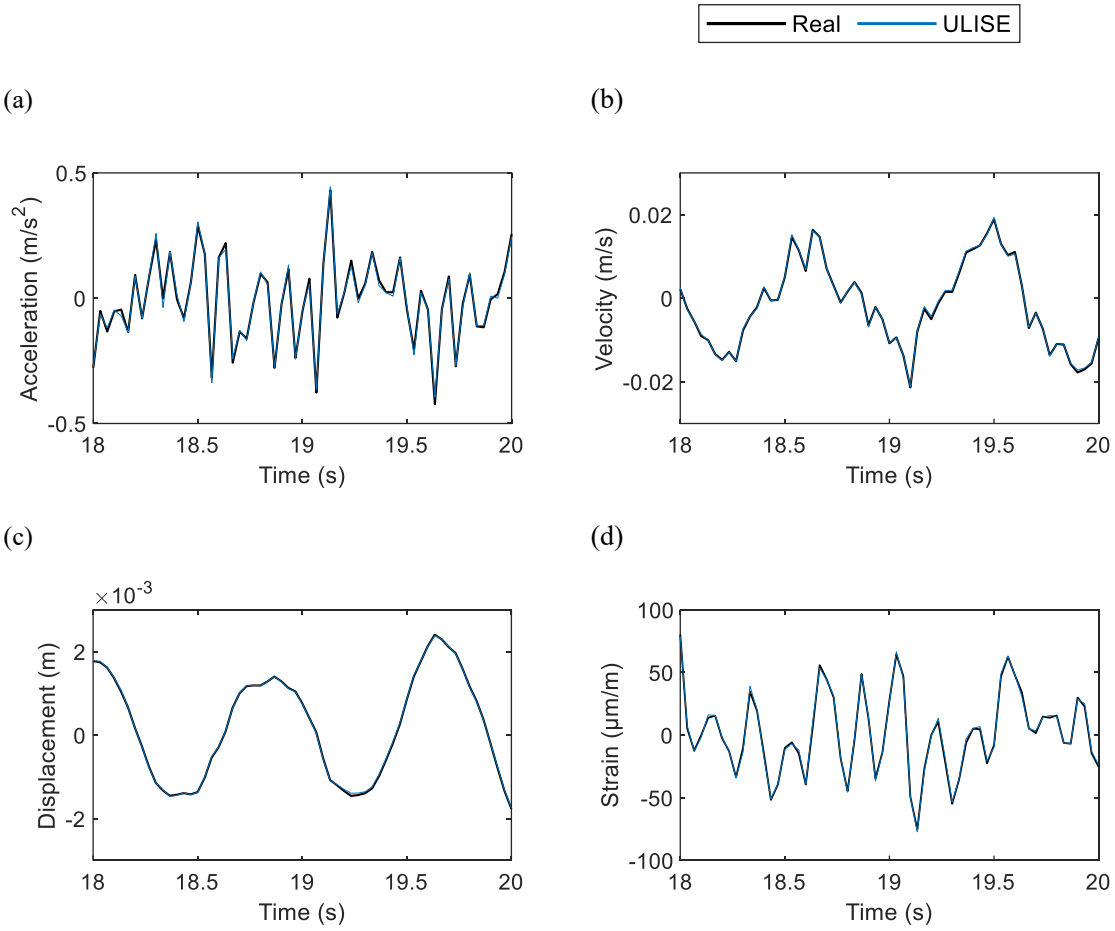

Fig. 5. ULISE-estimated time histories at DOF7 in Case 5: (a) acceleration, (b) velocity, (c) displacement, and (d) strain.

4.3 Non-collocated measurements

Collocated sensor arrangements are adopted in Cases 1-8, in which the locations with inputs are monitored by either accelerometers or strain gauges. This section evaluates the filter performance with non-collocated measurements in Case 9. The input and measurement noise are the same as those in Case 1. Among the three input locations (DOF2, DOF5, and DOF8), only DOF8 has an accelerometer, while other DOFs (DOF2 and DOF5) are not monitored by either accelerometer or strain gauges. The strain gauges are installed in stories 1, 3, and 6 to record the bending strain of the columns. The results shown in Fig. 6 show that the unknown excitations can be estimated even without the collocated acceleration or strain measurements. The reconstructed acceleration and strain responses at DOF7 are shown in **Fig. 7**, wherein no sensor is installed at DOF7 and the responses are estimated using the proposed ULISE iterations. The reconstructed acceleration and strain responses agree well with the real counterparts. Similar velocity and displacement reconstruction performances are omitted for brevity.

(a)

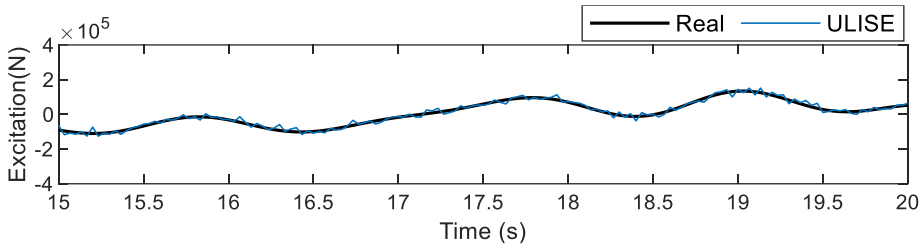

(b)

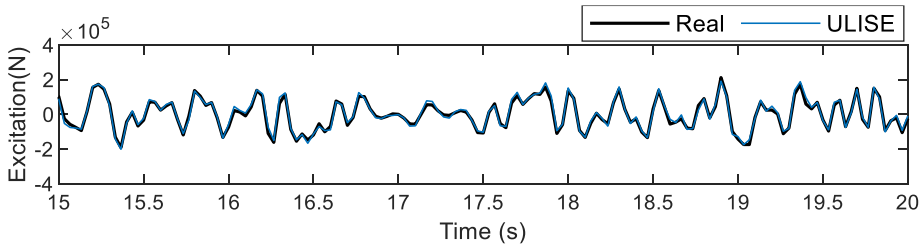

(c)

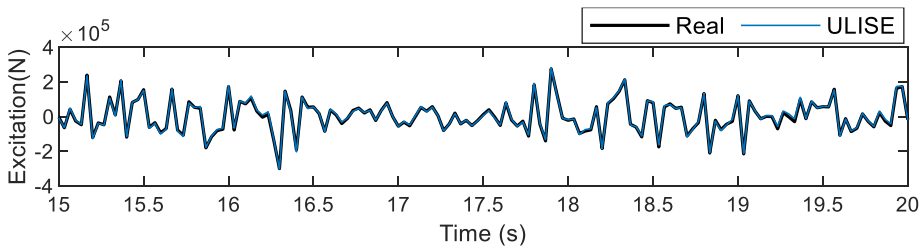

Fig. 6. ULISE-estimated time histories of excitations with non-collocated measurements at (a) DOF2, (b) DOF5, (c) and DOF8.

The results obtained in this subsection further verify the robustness and effectiveness of the proposed algorithm. The algorithm allows non-collocated sensor arrangement, and the system is still instantaneously invertible. This cannot be realized by the traditional KF-based joint input state estimators, which require acceleration measurements at unknown input locations [30].

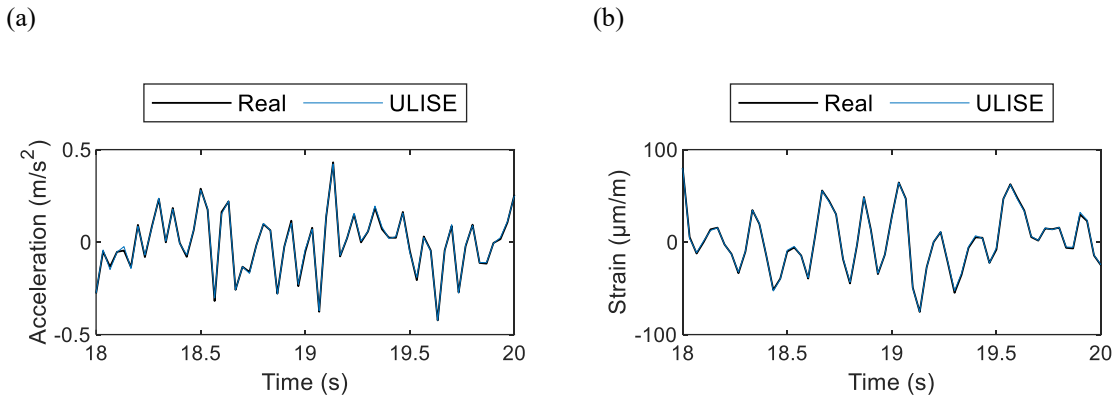

Fig. 7. Time history of the estimated responses with non-collocated measurements at DOF7 (a) acceleration, (b) strain.

5. Experimental validation

5.1 Experimental setup

A laboratory test on a five-story shear frame was conducted to verify the filter performances. The frame comprised five steel floor slabs with dimensions of 600 mm × 400 mm × 15 mm and four steel columns with a uniform cross section of 50 mm × 6 mm (**Fig. 8**). The total height of the frame was 1000 mm, and each floor had an equal height of 200 mm. Four oil dampers were installed to achieve structural damping close to those of real structures.

Two exciters were installed on the frame. An eccentric shaft wheel exciter with a controller (BXD120A-C, Oriental Motor, Japan) was placed on the roof, and an electromagnetic vibrator (LDS® V406, Brüel & Kjær, Denmark) was installed on the first floor of the frame to generate excitations. The floor displacements of the frame were recorded using four laser displacement transducers (LK-500, Keyence Corporation of America, USA), labeled sd2 to sd5 from floors 2 to 5. Five accelerometers

(TYPE 4533-B-002, Brüel & Kjær, Denmark) denoted as sa1 to sa5 were mounted on each floor. The excitation time history generated by the electromagnetic vibrator was recorded using a force sensor. The sampling frequency of the measurement system was set to 100 Hz. **Fig. 9** shows photographs of the laboratory test.

In this test, modal parameters were identified through hammer tests. The measured acceleration data were used in the experimental modal analysis by using the half-power bandwidth method. Model parameters (including the material density and Young's modulus) were updated to match the measured results by using the least square method. After model updating, the steel density was 7840kg/m^3, and Young's modulus was 231GPa. Notably, the updated Young's modulus indicated that the total stiffness of the steel frame was underestimated initially, which by no means implied that the steel frame was made of a material with a Young's modulus considerably higher than that of normal steel. As shown in **Table 6**, **t**he updated modal frequencies agreed well with the hammer test values.

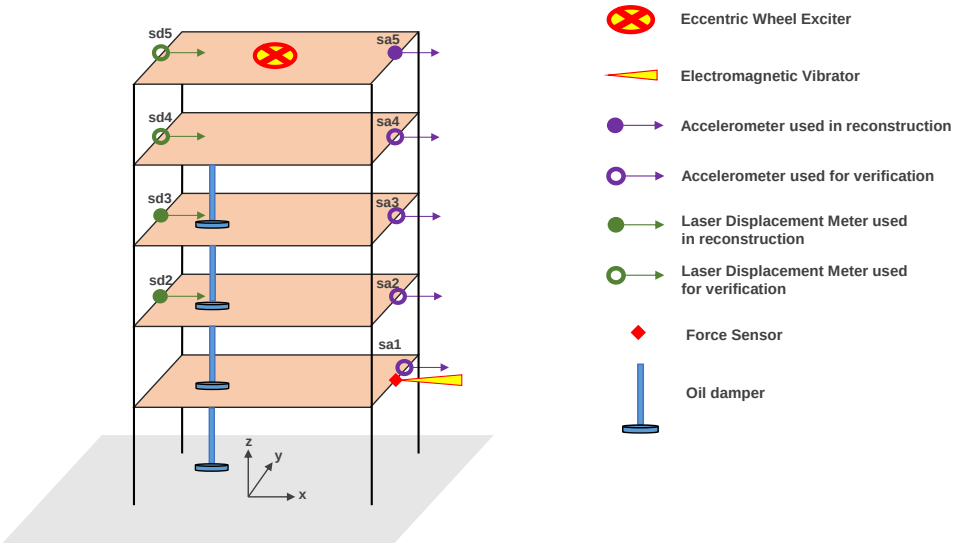

Fig. 8. Layout of the sensors and vibration exciter in the laboratory test.

Two tests were conducted to check the filter performances. In the first test, the lower electromagnetic vibrator generated a harmonic excitation with a frequency of 2 Hz. The top eccentric wheel exciter rotated at a speed of 600 rpm and applied another harmonic excitation with a frequency of 10 Hz on the top of the frame. In the second test, harmonic excitations with frequencies of 6 and 10.5 Hz were provided by the lower electromagnetic vibrator and the top eccentric vibrator, respectively. Not all of

the sensor measurements were used in the reconstruction algorithms. Response and input reconstruction were conducted using the acceleration recorded by accelerometer sa5 at DOF5 and the displacements recorded by sd2 at DOF2 and sd3 at DOF3. Filter performances were verified using measurements at other locations. The noise covariances for the acceleration measurement was $9\times10^{-5}\times\mathbf{I}_{n_{\text{acc}}}$, and for the displacement sensor was $3\times10^{-12}\times\mathbf{I}_{n_{\text{dis}}}$. The system noise covariance matrix was set as $\mathbf{Q}_k=10^{-20}\times\mathbf{I}$.

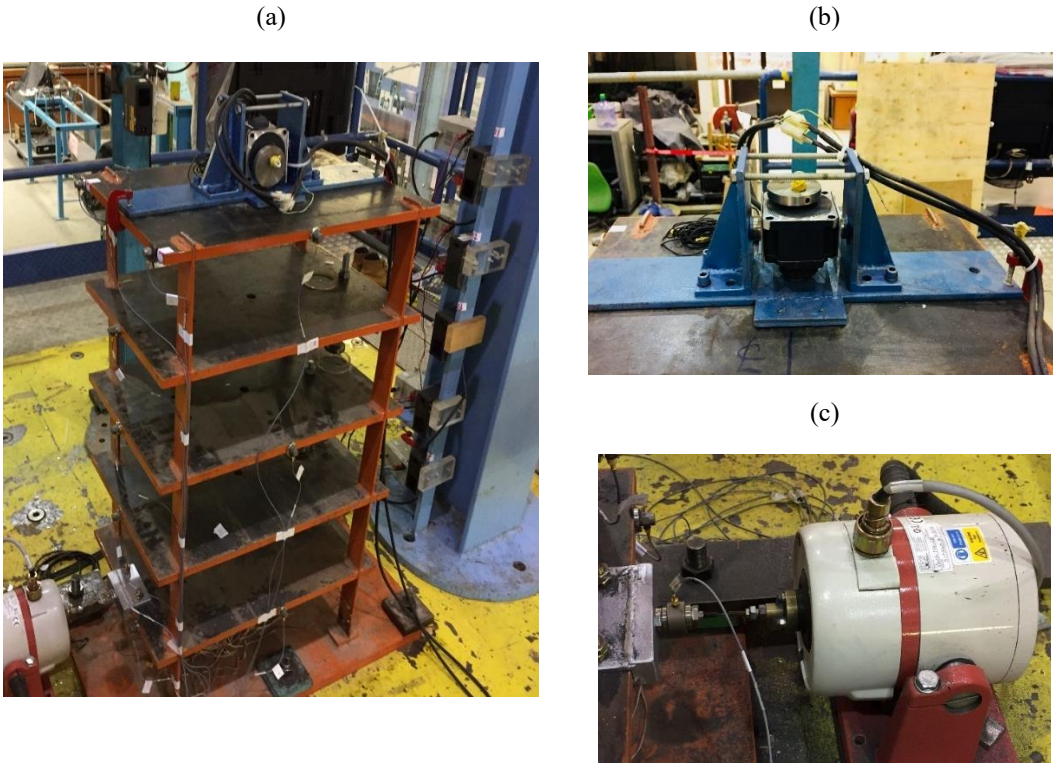

Fig. 9. Laboratory experimental setup: (a) whole setup, (b) eccentric shaft wheel exciter, and (c) electromagnetic vibrator.

Table 6

Frequencies and damping ratios of the tested frame

Vibration mode	1	2	3	4	5
Measured damping ratio (%)	0.85	0.56	0.51	0.46	0.60
Measured natural frequency (Hz)	8.79	26.07	42.48	56.40	66.65
Updated natural frequency (Hz)	8.79	26.18	42.30	55.42	63.96
Error of frequency (%)	0.00%	0.41%	−0.42%	−1.74%	−4.04%

For tests 1 and 2, the input estimations obtained using the proposed algorithm are shown in **Figs 10** and **11**, respectively. The inputs acting on DOF1 and DOF5 could be reconstructed using only one accelerometer (located at DOF5) in the ULISE. In GDF-II, acceleration measurement is necessary for input estimation. The input cannot be reconstructed without a collocated acceleration measurement. However, the input in the ULISE can be estimated even without an accelerometer. Nevertheless, the existence of an accelerometer will improve estimation accuracy. These results verify the capabilities of the ULISE algorithm to accommodate rank-deficient conditions in response reconstruction. For both the ULISE and GDF-II, normalization is required during data fusion for multi-type sensors. The normalization process can effectively prevent matrix ill-conditioned problems and guarantee filter convergence, and the lack of normalization can result in significant drift in input estimation.

(a)

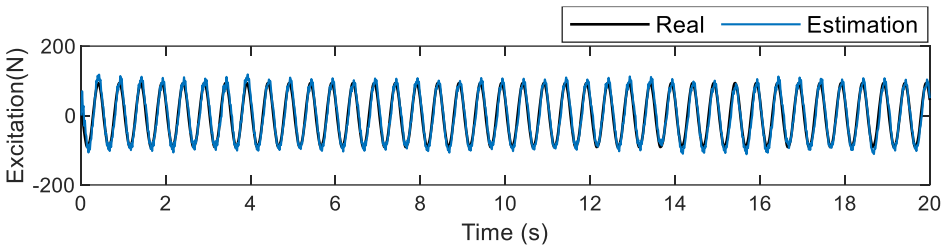

(b)

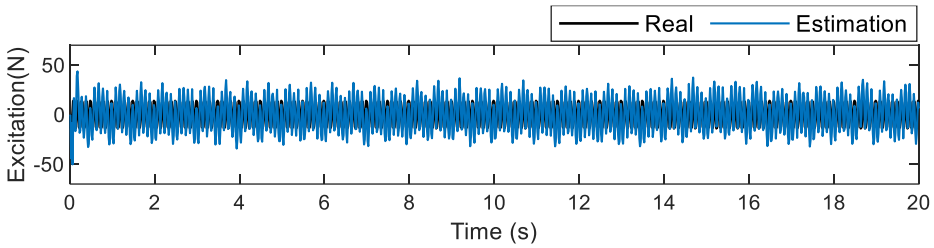

(c)

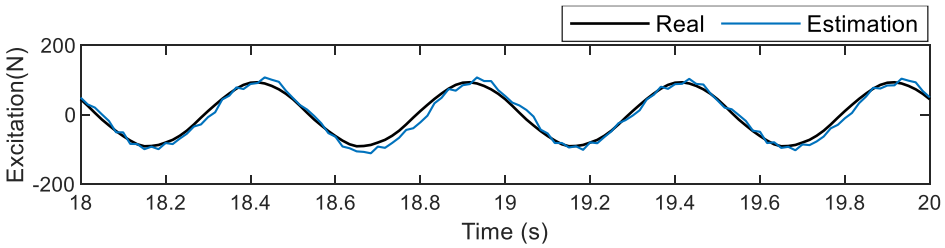

(d)

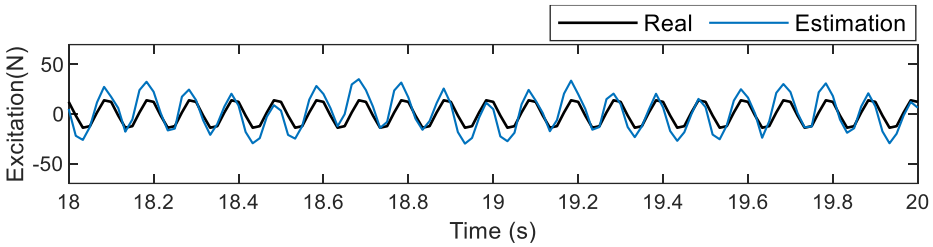

Fig. 10. Input estimations in Test 1: (a) estimated excitation at DOF1 (whole time history); (b) estimated excitation at DOF5 (whole time history); (c) estimated excitation at DOF1 (close view); (d) estimated excitation at DOF5 (close view).

(a)

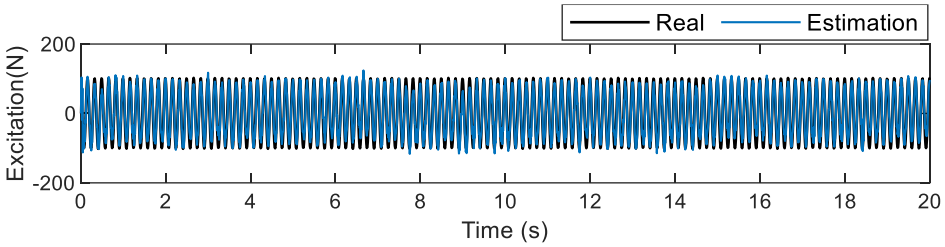

(b)

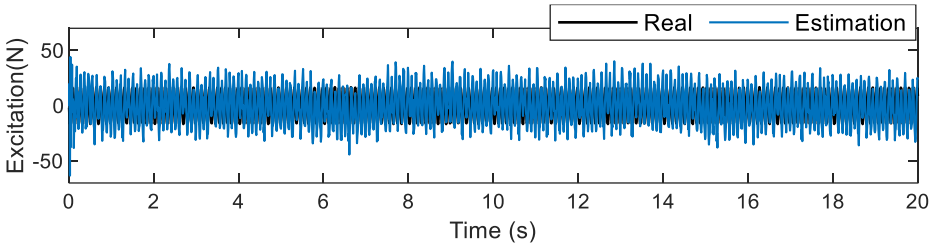

(c)

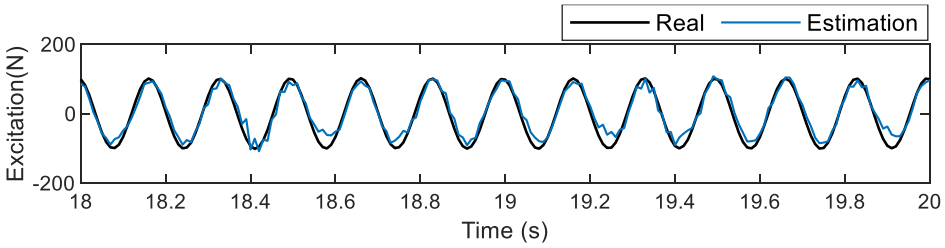

(d)

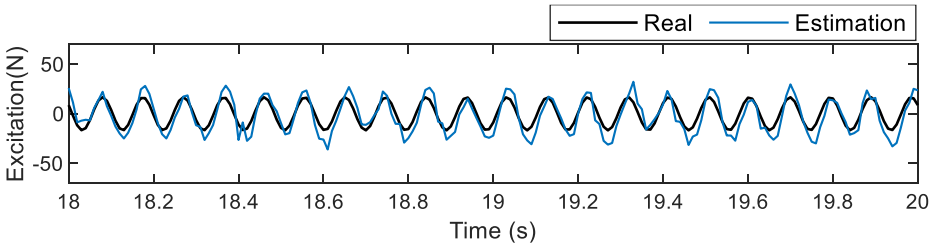

Fig. 11. Input estimations in Test 2: (a) estimated excitation at DOF1 (whole time history); (b)

estimated excitation at DOF5 (whole time history); (c) estimated excitation at DOF1 (close view); (d) estimated excitation at DOF5 (close view).

Figs. 12 and **13** present the ULISE-derived state (i.e., response) estimations for DOF4 in Tests 1 and 2. The estimated acceleration and displacement time histories were compared with the values measured by sensors sa4 and sd4. The displacement estimations agreed well with the measured data under rank-deficient conditions. However, some high-frequency oscillations occurred in the reconstructed acceleration time histories, attributable to the oscillations in the estimated input. The input estimation quality directly affects state estimation accuracy; therefore, obtaining accurate input estimations is important. These results also demonstrate the need to develop robust and accurate response reconstruction filters for SHM.

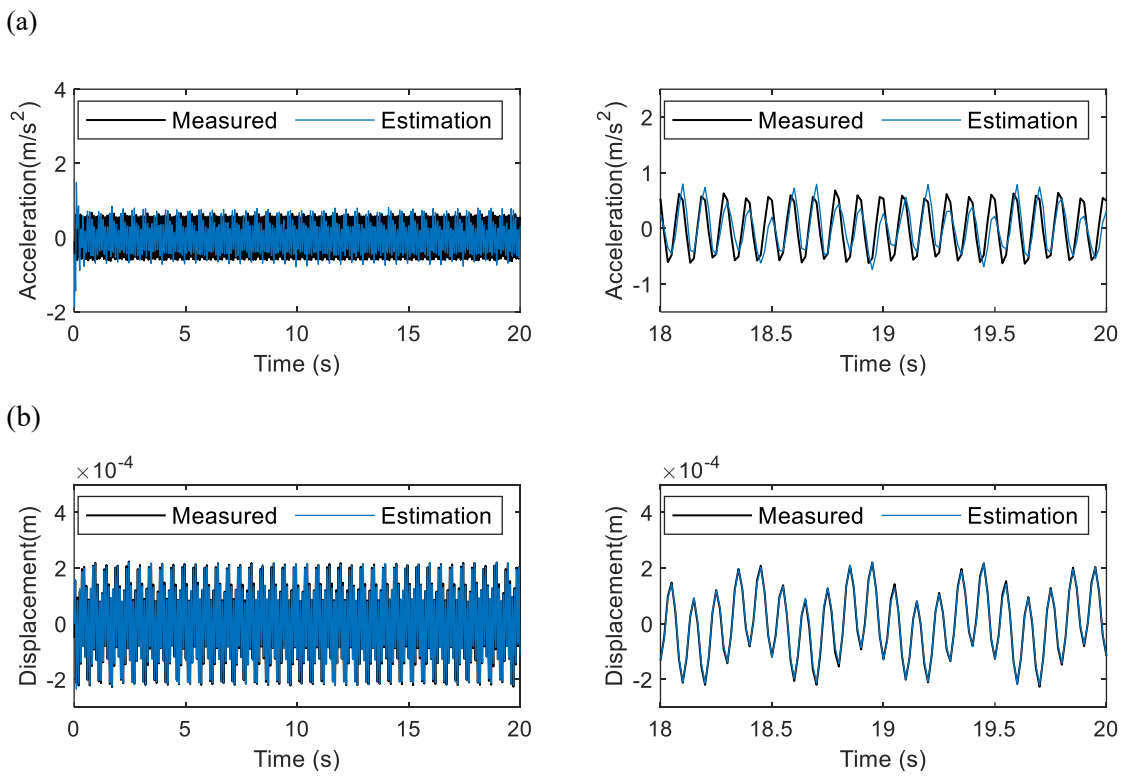

Fig. 12. State estimations for DOF4 in Test 1: (a) acceleration; (b) displacement.

(a)

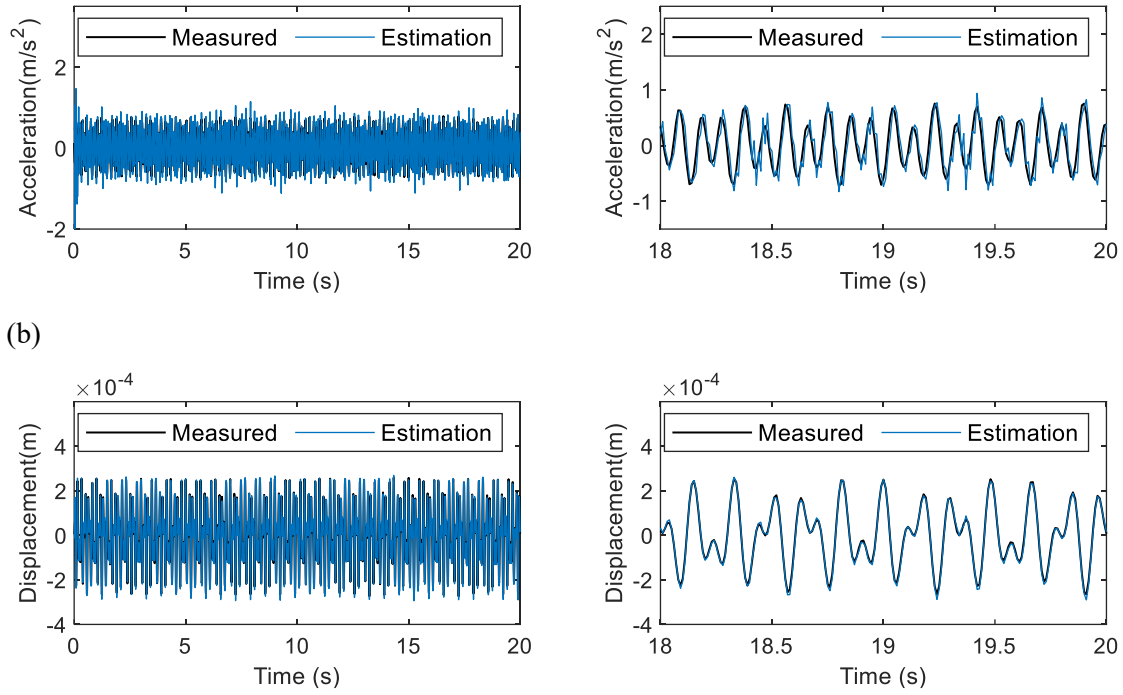

Fig. 13. State estimations for DOF4 in Test 2: (a) acceleration; (b) displacement.

6. Conclusions

In this study, a novel ULISE-based response reconstruction algorithm that does not require a full-rank direct feedthrough matrix is presented for the SHM of structures subjected to unknown dynamic loads for the first time. The algorithm can estimate the unknown inputs and state vectors without any prior assumption of the time histories of inputs. The algorithm does not require a full-rank system feedthrough matrix, which is necessary in the traditional GDF-II filter. Thus, the ULISE algorithm reduces the required number of accelerometers in real SHM applications and overcome one of the major limitations of the traditional methods. The effectiveness and advantages of the proposed ULISE-based structural response reconstruction algorithm were validated through numerical simulations and laboratory tests. The main conclusions of this study are encapsulated as follows:

1. The ULISE filter eliminates the full-rank requirement of the direct feedthrough matrix in response reconstruction, thereby overcoming the limitations of the traditional GDF-II filter.

2. The proposed ULISE-based response reconstruction method is identical to the traditional GDF-II under full-rank direct feedthrough matrix conditions. However, the presented algorithm can still provide satisfactory estimations based on incomplete acceleration measurements under rank-deficient direct feedthrough matrix conditions. Thus, the ULISE filter can be regarded as a generalized and improved

version of the two traditional GDF filters.

3. The proposed ULISE filter can directly fuse displacement and acceleration measurements at time k and improve input estimation through a two-step approach under rank-deficient conditions.

4. The collocated sensor arrangement is no longer necessary in the proposed ULISE algorithm. Satisfactory joint input and state estimations results could be achieved even if the input locations are not monitored by any sensors.

5. Similar to traditional GDF filters, the ULISE-based algorithm is sensitive to measurement noise. It is interesting to note that although the input estimation has significant errors in one extreme case, the state reconstruction can still benefit from the input reconstruction.

The results of this study demonstrate the great potential of the ULISE filter algorithm for response reconstruction in various scenarios. Nevertheless, only laboratory experiments were conducted in this study, and the applications of the ULISE to real-world, large-scale civil structures will be investigated in the future to further demonstrate the practicability of the filter.

Acknowledgments

The authors acknowledge financial support from the Research Grants Council of Hong Kong through the Research Impact Fund (PolyU R5020-18) and Theme-based Research Scheme (T22-502/18-R), the Hong Kong Branch of the National Rail Transit Electrification and Automation Engineering Technology Research Center (No. K-BBY1), and The Hong Kong Polytechnic University (ZE2L, ZVX6, BBW8).

Appendix A. Excitation estimation results in Cases 6-8 in the numerical simulations

The reconstructed time histories of the inputs in numerical Case 5 are presented in Section 4.2. The reconstructed inputs in Cases 6-8 are not discussed in the paper and thus are presented in this appendix as supplementary materials.

(a)

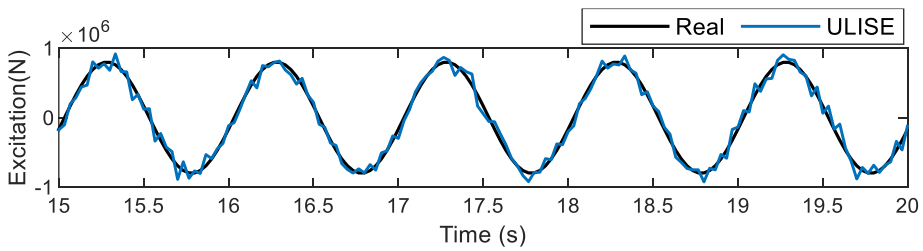

(b)

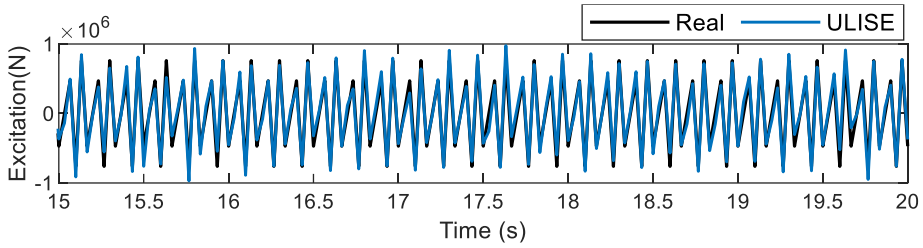

(c)

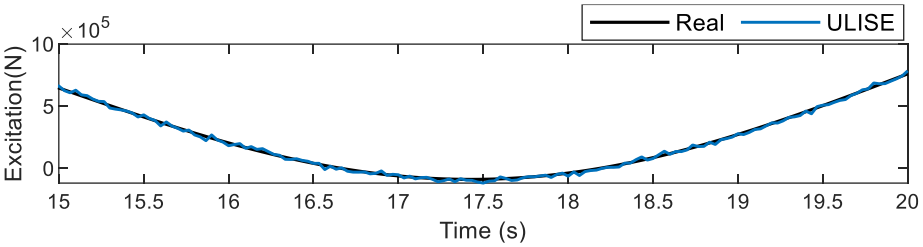

Fig. A1. Close view of the time histories of the estimated input excitations in Case 6 (a) at DOF2, (b) at DOF5, (c) at DOF8.

(a)

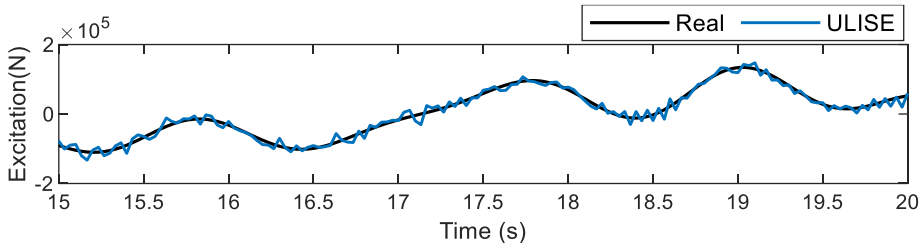

(b)

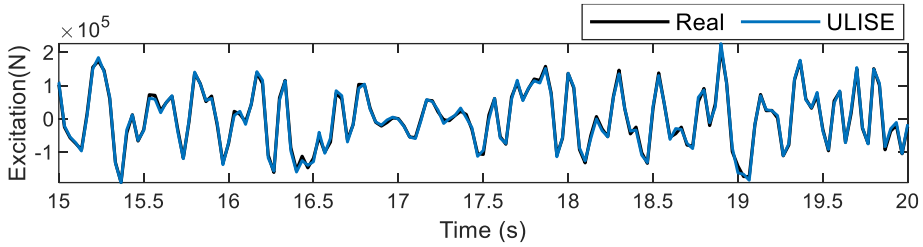

(c)

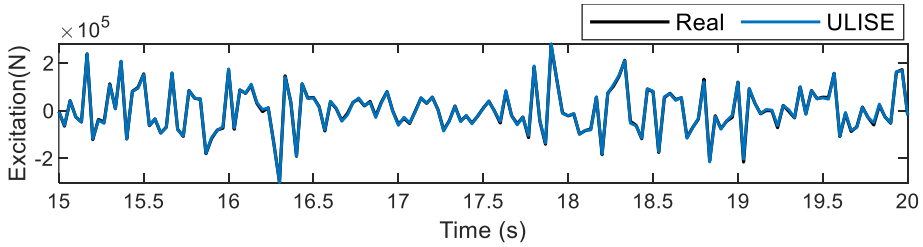

Fig. A2. Close view of the time histories of the estimated input excitations in Case 7 (a) at DOF2,

(b) at DOF5, (c) at DOF8.

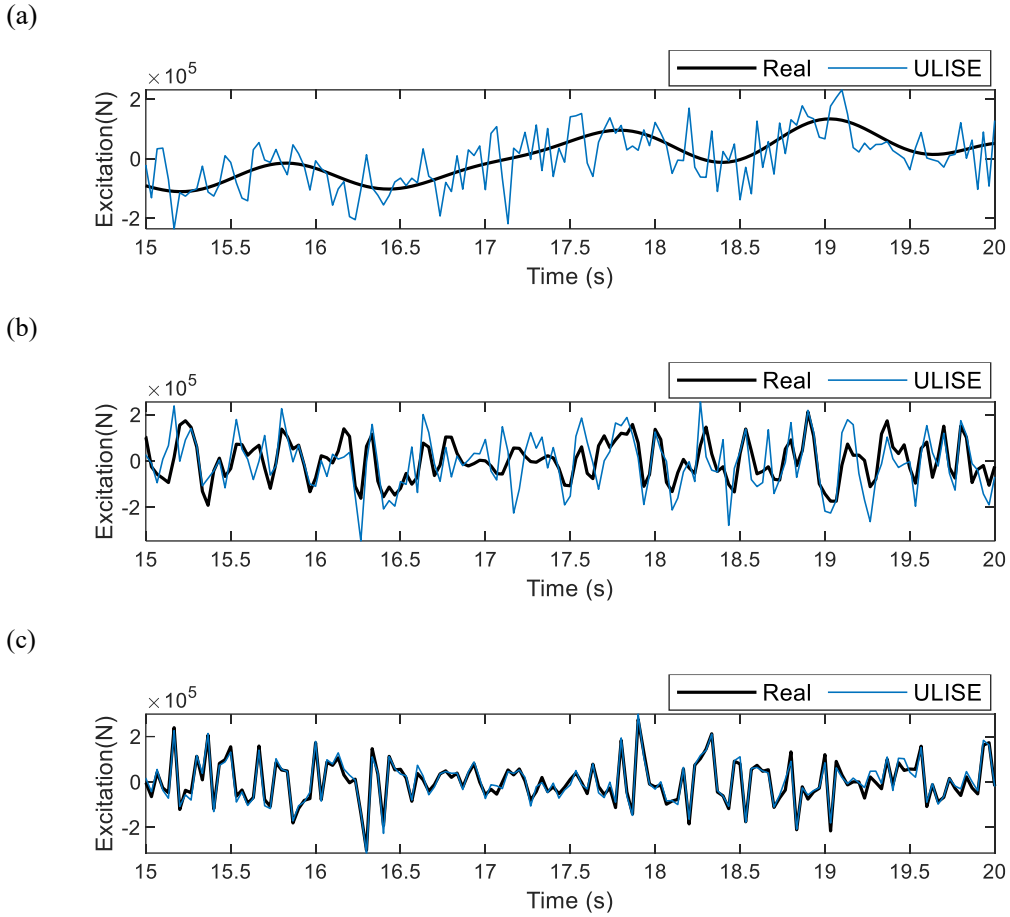

Fig. A3. Close view of the time histories of estimated input excitation in Case 8 (a) at DOF2, (b) at DOF5, (c) at DOF8.

References

1. S. Li, S. Zhu, Y. L. Xu, Z. W. Chen, H. Li, Long-term condition assessment of suspenders under traffic loads based on structural monitoring system: Application to the Tsing Ma Bridge, Struct Control Health Monit 19(1) (2012) 82-101. https://doi.org/10.1002/stc.427.
2. Y.L. Xu, Y. Xia, Structural health monitoring of long-span suspension bridges, CRC Press, 2011.
3. D.C. Kammer, Estimation of structural response using remote sensor locations, J Guid Control Dyn **20**(3) (1997) 501-508. https://doi.org/10.2514/2.4069.
4. W. Liu, D. Ewins, Transmissibility properties of MDOF systems, SPIE proceedings series (1998) 847-854
5. N.E. Huang, Z. Shen, S. R. Long, M. C. Wu, H. H. Shih, Q. Zheng, N. C. Yen, C. C. Tung, H. H. Liu, The empirical mode decomposition and the Hilbert spectrum for nonlinear and non-stationary time series analysis, Proceedings of the Royal Society of London. Series A: mathematical, physical and engineering

sciences **454**(1971) (1998) 903-995. https://doi.org/10.1098/rspa.1998.0193.

6. J. He, X. Guan, Y. Liu, Structural response reconstruction based on empirical mode decomposition in time domain, Mech Syst Signal Process **28** (2012) 348-366. https://doi.org/10.1016/j.ymssp.2011.12.010.
7. G. Ambrosino, G. Celentano, R. Setola, A spline approach to state reconstruction for optimal active vibration control of flexible systems, Proceedings of International Conference on Control Applications, IEEE, (1995) 896-901. https://doi.org/10.1109/CCA.1995.555873.
8. R. Setola, A spline-based state reconstruction for active vibration control of a flexible beam, J. Sound Vib. **213**(5) (1998) 777-790. https://doi.org/10.1006/jsvi.1998.1531.
9. M. P. Limongelli, Optimal location of sensors for reconstruction of seismic responses through spline function interpolation, Earthq Eng Struct Dyn **32**(7) (2003) 1055-1074. https://doi.org/10.1002/eqe.262.
10. R. E. Kalman, A new approach to linear filtering and prediction problems. 1960.
11. S. Zhu, X. H. Zhang, Y. L. Xu, S. Zhan, Multi-type sensor placement for multi-scale response reconstruction, Adv. Struct. Eng. **16**(10) (2013) 1779-1797. https://doi.org/10.1260/1369-4332.16.10.1779.
12. X. H. Zhang, Y. L. Xu, S. Zhu, S. Zhan, Dual-type sensor placement for multi-scale response reconstruction, Mechatronics **24**(4) (2014) 376-384. https://doi.org/10.1016/j.mechatronics.2013.05.007.
13. X. H. Zhang, S. Zhu, Y. L. Xu, X. J. Homg, Integrated optimal placement of displacement transducers and strain gauges for better estimation of structural response, Int. J. Struct. Stab. Dyn. **11**(03) (2011) 581-602. https://doi.org/10.1142/S0219455411004221.
14. Y. L. Xu, X. H. Zhang, S. Zhu, S. Zhan, Multi-type sensor placement and response reconstruction for structural health monitoring of long-span suspension bridges, Sci. Bull. 61(4) (2016) 313-329. https://doi.org/10.1007/s11434-016-1000-7.
15. V. Aidala, S. Hammel, Utilization of modified polar coordinates for bearings-only tracking, IEEE Trans. Automat. Contr. **28**(3) (1983) 283-294. https://doi.org/10.1109/TAC.1983.1103230
16. Y. Lei, H. Zhou, Z.L. Lai, A computationally efficient algorithm for real-time tracking the abrupt stiffness degradations of structural elements, COMPUT-AIDED CIV INF **31**(6) (2016) 465-480. https://doi.org/10.1111/mice.12217.
17. R. Nayek, S. Chakraborty, S. Narasimhan, A Gaussian process latent force model for joint input-state estimation in linear structural systems, Mech. Syst. Signal Process. 128 (2019) 497–530. https://doi.org/10.1016/j.ymssp.2019.03.048
18. E. Lourens, E. Reynders, G. De Roeck, G. Degrande, G. Lombaert, An augmented Kalman filter for force identification in structural dynamics, Mech Syst Signal Process **27** (2012) 446-460. https://doi.org/10.1016/j.ymssp.2011.09.025.
19. M. Aucejo., O. De Smet, J.-F. Deü, Practical issues on the applicability of Kalman filtering for reconstructing mechanical sources in structural dynamics, J. Sound Vib. **442** (2019) 45-70. https://doi.org/10.1016/j.jsv.2018.10.060.
20. F. Naets, J. Cuadrado, W. Desmet, Stable force identification in structural dynamics using Kalman filtering and dummy-measurements, Mech Syst Signal Process **50** (2015) 235-248. https://doi.org/10.1016/j.ymssp.2014.05.042.

21. V.K. Dertimanis, E.N. Chatzi, S. Eftekhar Azam, C. Papadimitriou, Input-state-parameter estimation of structural systems from limited output information, Mech. Syst. Signal Process. 126 (2019) 711–746.22. https://doi.org/10.1016/j.ymssp.2019.02.040
22. K.E. Tatsis, K. Agathos, E. N. Chatzi, V. K. Dertimanis, A hierarchical output-only Bayesian approach for online vibration-based crack detection using parametric reduced-order models, Mech. Syst. Signal Process. 167 (2022) 108558. https://doi.org/10.1016/j.ymssp.2021.108558
23. P. K. Kitanidis, Unbiased minimum-variance linear state estimation, Automatica 23(6) (1987) 775-778. https://doi.org/10.1016/0005-1098(87)90037-9.
24. C. S. Hsieh, Robust two-stage Kalman filters for systems with unknown inputs, IEEE Trans. Automat. Contr. **45**(12) (2000). https://doi.org/2374-2378. 10.1109/9.895577.
25. S. Gillijns, B. De Moor, Unbiased minimum-variance input and state estimation for linear discrete-time systems, Automatica **43**(1) (2007) 111-116. https://doi.org/10.1016/j.automatica.2006.08.002.
26. S. Gillijns, B. De Moor, Unbiased minimum-variance input and state estimation for linear discrete-time systems with direct feedthrough, Automatica **43**(5) (2007) 934-937. https://doi.org/10.1016/j.automatica.2006.11.016.
27. E. Lourens, C. Papadimitriou, S. Gillijns, E. Reynders, G. De Roeck, G. Lombaert, Joint input-response estimation for structural systems based on reduced-order models and vibration data from a limited number of sensors, Mech Syst Signal Process **29** (2012) 310-327. https://doi.org/10.1016/j.ymssp.2012.01.011.
28. K. Maes, A. W. Smyth, G. De Roeck, G. Lombaert, Joint input-state estimation in structural dynamics, Mech Syst Signal Process **70** (2016) 445-466. https://doi.org/10.1016/j.ymssp.2015.07.025.
29. K. Maes, S. Gillijns, G. Lombaert, A smoothing algorithm for joint input-state estimation in structural dynamics, Mech. Syst. Signal Process. 98 (2018)292–309. https://doi.org/10.1016/j.ymssp.2017.04.047
30. K. Maes, E. Lourens, K. Van Nimmen, E. Reynders, G. De Roeck, G. Lombaert, Design of sensor networks for instantaneous inversion of modally reduced order models in structural dynamics, Mech Syst Signal Process **52** (2012) 628-644. https://doi.org/10.1016/j.ymssp.2014.07.018.
31. S. Z. Yong, M. Zhu, E. Frazzoli, A unified filter for simultaneous input and state estimation of linear discrete-time stochastic systems, Automatica **63** (2016) 321-329. https://doi.org/10.1016/j.automatica.2015.10.040.
32. C. S. Hsieh, Extension of unbiased minimum-variance input and state estimation for systems with unknown inputs. Automatica **45**(9) (2009) 2149-2153. https://doi.org/10.1016/j.automatica.2009.05.004.
33. Y. Cheng, H. Ye, Y. Wang, & D. Zhou, Unbiased minimum-variance state estimation for linear systems with unknown input, Automatica 45(2) (2009) 485-491. https://doi.org/10.1016/j.automatica.2008.08.009.
34. R. A. De Callafon, B. Moaveni, J. P. Conte, X. He, E. Udd, General realization algorithm for modal identification of linear dynamic systems, J Eng Mech **134**(9) (2008) 712-722. https://doi.org/10.1061/(ASCE)0733-9399(2008)134:9(712).
35. S. R. Azam, E. Chatzi, C. Papadimitriou, A dual Kalman filter approach for state estimation via output-

only acceleration measurements, Mech Syst Signal Process **60** (2015) 866-886. https://doi.org/10.1016/j.ymssp.2015.02.001.